Phenology and time series trends of the dominant seasonal phytoplankton bloom across global scales

Kevin D. Friedland[1,*], Colleen B. Mouw[2], Rebecca G. Asch[3,4], A. Sofia A. Ferreira[5], Stephanie Henson[6], Kimberly J. W. Hyde[1], Ryan E. Morse[1], Andrew C. Thomas[7], Damian C. Brady[7]

[1]National Marine Fisheries Service, 28 Tarzwell Dr., Narragansett, RI 02882, USA
[2]University of Rhode Island, Graduate School of Oceanography, 215 South Ferry Road, Narragansett, RI 02882, USA
[3] Princeton University, Program in Atmospheric and Oceanic Sciences, 300 Forrestal Road, Princeton, NJ 08540, USA
[4] Current address: East Carolina University, Department of Biology, 1000 East 5th Street, Greenville, NC 27858, USA
[5]School of Oceanography, University of Washington, Seattle, WA, USA
[6]National Oceanography Centre, European Way, Southampton, UK
[7]School of Marine Sciences, University of Maine, Orono, ME, USA

Kevin D. Friedland (kevin.friedland@noaa.gov)
Colleen B. Mouw (cmouw@uri.edu)
Rebecca G. Asch (aschr16@ecu.edu)
A. Sofia A. Ferreira (asofiaaferreira@gmail.com)
Stephanie Henson (S.Henson@noc.ac.uk)
Kimberly J. W. Hyde (kimberly.hyde@noaa.gov)
Ryan E. Morse (ryan.morse@noaa.gov)
Andrew C. Thomas (thomas@maine.edu)
Damian C. Brady (damian.brady@maine.edu)

*Correspondence: Kevin Friedland, National Marine Fisheries Service, 28 Tarzwell Dr., Narragansett, RI 02882, USA, E-mail: kevin.friedland@noaa.gov

Number of words in the Abstract: 291

Number of words in main body of the paper: 8396

Number of references: 87

Running head: Global Bloom Phenology

ABSTRACT

Aim This study examined phytoplankton blooms on a global scale with the intention of describing patterns of bloom timing and size, the effect of bloom timing on the size of blooms, and time series trends in bloom characteristics.

Location Global.

Methods We used a change-point statistics algorithm to detect phytoplankton blooms in time series of chlorophyll concentration data over a global grid. At each study location, the bloom statistics for the dominant bloom, based on the search time period that resulted in the most blooms detected, were used to describe the spatial distribution of bloom characteristics over the globe. Time series of bloom characteristics were also subjected to trend analysis to describe regional and global change in bloom timing and size.

Results The characteristics of the dominant bloom were found to vary with latitude and in localized patterns associated with specific oceanographic features. Bloom timing had the most profound effect on bloom duration, with early blooms tending to last longer than later starting blooms. Time series of bloom timing and duration were trended, suggesting blooms have been starting earlier and lasting longer, respectively, on a global scale. Blooms have also increased in size at high latitudes and decreased in equatorial areas based on multiple size metrics.

Main conclusions Phytoplankton blooms have changed on both regional and global scales, which has ramifications for the function of food webs providing ecosystem services. A tendency for blooms to start earlier and last longer will have an impact on energy flow pathways in ecosystems, differentially favoring the productivity of different species groups. These changes may also affect the sequestration of carbon in ocean ecosystems. A shift to earlier bloom timing is consistent with the expected effect of warming ocean climate conditions observed in recent decades.

INTRODUCTION

Primary production in the oceans accounts for approximately half of the carbon fixed by photosynthesis on a global scale (Field *et al.*, 1998). This production fuels the growth and reproduction of living marine resources and is a critical factor exerting control over which species produce harvestable surpluses, contributing to fishery yields (Ryther, 1969; Chassot *et al.*, 2010; Stock *et al.*, 2017) and ensuring global food security (Perry, 2011; Christensen *et al.*, 2015). In addition to the production of continental shelf species that are exploited in fisheries, there is also significant trophic transfer between open ocean primary production and mesopelagic fishes on a global basis (Davison *et al.*, 2013; Irigoien *et al.*, 2014). At a more fundamental level, phytoplankton production is the central driver of most marine ecosystems (Sigman & Hain, 2012) and the biogeochemical processes governing carbon flow and export flux (Doney *et al.*, 2014; Laufkotter *et al.*, 2016). However, oceanic photosynthetic production is not constant in time and space; geographic and phenological (bloom timing and duration) variability occurs due to complex biophysical factors controlling phytoplankton blooms owing to the dynamics between the rates of cell reproduction and mortality associated with death and grazing (Behrenfeld & Boss, 2014; Cherkasheva *et al.*, 2014). The variability in blooms affect energy flow from phytoplankton production to pelagic and demersal communities and thus both horizontal and vertical transport of energy in the water column (Corbiere *et al.*, 2007).

Phytoplankton bloom dynamics have been characterized on basin and global scales, identifying differing patterns of bloom phenology by latitude and oceanic province. Analyses of time series change in bloom dynamics complement descriptions of the spatial organization of blooms utilizing a number of different sources of data. For example, a study with a geographic focus in the North Atlantic found that spring bloom timing has advanced for some temperate latitude regions and was delayed in other areas, whereas the fall and winter blooms have been mostly delayed (Taboada & Anadon, 2014). Other longer-term studies identified the effects of changing mixed layer dynamics on the relative strength of spring and fall blooms in the North Atlantic (Martinez *et al.*, 2011) and widespread shifts in bloom phenology associated with broad-scale changes in the coupled atmosphere-ocean system (D'Ortenzio *et al.*, 2012). Some of the most dramatic changes in bloom characteristics and phenology have occurred in the Arctic, where bloom maximums have advanced on the order of fifty days from 1997 to 2009 as a consequence of changes in seasonal ice cover (Kahru *et al.*, 2011). Changes in bloom magnitude and timing alter energy flow in the ecosystem, which in turn impact the growth and reproduction of higher trophic levels in the food web (Cushing, 1990; Hunt *et al.*, 2002; Platt *et al.*, 2003; Schweigert *et al.*, 2013; Malick *et al.*, 2015).

101   Climate variation can indirectly modify bloom timing and size through mechanisms that
102   influence water column conditions such as the supply and ratio of nutrients and light availability. As
103   climate systems shift in response to anthropogenic forcing, there is a need to understand their impact
104   on bloom dynamics both retrospectively and in a forecasting context. As an example, in the Baltic Sea,
105   investigators found that bloom duration has increased in recent years and associated this change in
106   bloom dynamics to increasing water temperature and declining wind stress, which they attributed to
107   global climate change (Groetsch *et al.*, 2016). Change in climate conditions may act to modify blooms
108   through the direct effects of nutrient supply and grazing; additionally, changing distributions of parasites
109   and viruses associated with climate change will likely play a larger role in the dynamics of blooms and
110   the nature of fixed carbon available to primary grazers (Frenken *et al.*, 2016). Projections of bloom
111   dynamics by global earth system models (e.g., CanESM2, GFDL-ESM2M, HadGEM2-CC, IPSL-CM5A-MR,
112   MPI-ESM-LR, and NEMO-MEDUSA) suggest that regions dominated by seasonal blooms may see
113   diminished bloom events that are replaced by smaller seasonal blooms more typical of contemporary
114   subtropical regions (Henson *et al.*, 2013). Other simulations suggest that future climate will greatly
115   change the nature of seasonal and permanent stratification features, which is one of the more
116   important physical factors controlling the onset and duration of blooms (Holt *et al.*, 2016). Furthermore,
117   direct temperature effects on cell division rates and physiological processes could also influence bloom
118   timing in a warming climate (Hunter-Cevera *et al.*, 2016).
119   In this manuscript we describe the spatial and temporal dynamics of the dominant
120   phytoplankton blooms of the global ocean. While phytoplankton phenology has been actively
121   investigated, here we define events detected using change-point statistics (Friedland *et al.*, 2015;
122   Friedland *et al.*, 2016) as opposed to other frequently used algorithms which generally rely on threshold
123   methods and curve fitting (Ueyama & Monger, 2005; Ji *et al.*, 2010; Brody *et al.*, 2013; Blondeau-
124   Patissier *et al.*, 2014; Marchese *et al.*, 2017). Furthermore, many of these methods rely on the
125   availability of a full yearly cycle of data, which limits their application at high latitudes due to the missing
126   winter values from satellite data (Cole *et al.*, 2012; Ferreira *et al.*, 2014; Ferreira *et al.*, 2015); noting
127   however, that productive approaches to deal with this issue are emerging (Marchese *et al.*, 2017). The
128   change-point approach provides distinct determinations of bloom start and end, which allows
129   exploration of the internal relationships among bloom characteristics, and represents an area of novelty
130   compared to previous analyses of global, satellite-derived trends in phytoplankton phenology (Kahru *et*
131   *al.*, 2011; Racault *et al.*, 2012). As will be the case with subsequent analyses, our time series is longer
132   than those used by these previous studies, thus statistics of association and trend are informed by more

133   data. Using this more mature remote sensing ocean color time series, our analysis examines times series

134   trends in bloom parameters on both regional and global scales, with summary data for specific

135   latitudinal ranges.

136

137

138   **METHODS**

139

140   **Chlorophyll data**

141   We analyzed phytoplankton blooms using chlorophyll *a* concentration ([Chl]) data extracted from

142   remote-sensing databases using a global 1° latitudinal/longitudinal grid centered on half degrees. [Chl]

143   was based on measurements made with the Sea-viewing Wide Field of View Sensor (SeaWiFS),

144   Moderate Resolution Imaging Spectroradiometer on the Aqua satellite (MODIS), Medium Resolution

145   Imaging Spectrometer (MERIS), and Visible and Infrared Imaging/Radiometer Suite (VIIRS) sensors. We

146   used the Garver, Siegel, Maritorena Model (GSM) merged data product at 100 km (equivalent to a 1°

147   grid) and 8-day spatial and temporal resolutions, respectively, obtained from the Hermes GlobColour

148   website (hermes.acri.fr/index.php). These four sensors provide an overlapping time series of [Chl]

149   during the period 1998 to 2015 and were combined based on a bio-optical model inversion algorithm

150   (Maritorena *et al.*, 2010). The compiled time series from January 1, 1998 to December 27, 2015,

151   consisted of 828 8-day [Chl] observations for each grid location. There were 38,433 grid locations with

152   sufficient [Chl] to perform at least one bloom determination (at least one run of 23 time steps with 12

153   [Chl] observations), including some locations that were in inland waters which did not factor into the

154   analysis. Some aspects of the analysis do not include data from high latitudes (>62° N/S) due to the

155   increased frequency of gaps at these latitudes reflecting the limited period of available data during the

156   year and the presence of sea ice and cloud cover, which both obscure ocean color satellite imagery.

157

158   **Dominant plankton bloom analyses**

159   Seasonal phytoplankton blooms, as evidenced by changes in [Chl], were detected using change-point

160   statistics. In this study, we define a seasonal bloom as a discernable elevation in [Chl], one that is

161   bracketed by distinct start and end points as identified using the change-point algorithm, occurring

162   within a 6-month time frame. For each grid location, the search for bloom events started with the first

163   half-year block of the time series (the first 23 8-day [Chl] measurements), progresses to search for

164   blooms during the next half-year block beginning with the second [Chl] measurement of the year, and

5

165   then continues to step through the entire time series. Only half-year series with a minimum of 12

166   observations were considered for analysis; linear interpolation was used to fill missing values within the

167   range of the data and missing values outside the range were filled with the first and last observations at

168   the beginning or end of the time series, respectively. Hence, for each grid location, 806 bloom

169   determinations were attempted and each detected bloom was associated with one of the 46 search

170   start days of the year (46 bloom detections over the first 17 years of the times series and 24 attempts in

171   the final year). From these data, we identified the search start day of the year that yielded the dominant

172   bloom, which was defined as the search window that yielded the highest number of bloom detections. If

173   more than one start day yielded the highest number of bloom detections, the dates were sorted

174   sequentially and the median day was used as the dominant bloom. With the 38,433 grid locations and

175   factoring 806 bloom determinations per location, ~31 million bloom determinations were attempted.

176   Blooms were detected using the sequential averaging algorithm called STARS or "sequential *t*-

177   test analysis of regime shifts" (Rodionov, 2004, 2006) which finds the change-points in a time series.

178   STARS algorithm parameters were specified *a priori*: the alpha level used to test for a change in the

179   mean was set to $\alpha = 0.1$; the length criteria, the number of time steps to use when calculating the mean

180   level of a new regime, was set to 5; and, the Huber weight parameter, which determines the relative

181   weighting of outliers in the calculation of the regime mean, was set to 3. A bloom was considered to

182   have occurred if there was a period bracketed by a positive and negative change-point. We ignored

183   change-points (positive or negative) that occurred in the first or last two periods of the time series (8-

184   day periods 1, 2, 22 and 23). The minimum duration of a bloom was three sample periods, which

185   represents the minimum span the algorithm needed to find a positive followed by a negative change-

186   point. This method has been used in previous analyses of US Northeast Shelf (Friedland *et al.*, 2008;

187   Friedland *et al.*, 2015), Arctic (Friedland & Todd, 2012), and North Atlantic bloom patterns (Friedland *et*

188   *al.*, 2016).

189   We extracted a suite of statistics to characterize the timing and size of each bloom event. For

190   each location, we calculated bloom frequency as the percentage of years with a detected bloom in study

191   years with sufficient data to do a bloom determination, i.e. some locations may have had persistent

192   cloud cover in a year so a bloom detection could not be attempted. Bloom start was defined as the first

193   day of the year of the bloom period. Bloom duration was defined as the number of days of the bloom

194   period. Bloom intensity was the mean of the [Chl] during the bloom period which carries the unit mg m^{-3}

195   and reflects the biomass of the bloom. Bloom magnitude was the integral of the [Chl] during the bloom

196   period and describes the overall size of the event considering that short and long duration blooms can

197   have the same intensity. Magnitude can be calculated as the sum of the [Chl] during the blooms, which

198   carries the unit mg m^{-3}; or, as the product of the mean [Chl] during the bloom and the duration in 8-day

199   periods, which carries the unit mg m^{-3} 8-day. We used the latter unit designation to distinguish it from

200   bloom intensity.

201

202   **Effect of bloom timing on bloom characteristics**

203   For each grid location, we examined the correlation between bloom start and duration, magnitude, and

204   intensity of the dominant bloom. Pearson product-moment correlations were calculated and limited to

205   grid locations with a minimum of eight detected blooms. Significant correlations with a probability level

206   α <0.05 were highlighted in global maps. Given that regressions were performed on a grid cell-by-cell

207   basis, it is possible that multiple testing could have led to excess accumulation of Type I error. However,

208   spatial patterns shown herein generally remain consistent if a different threshold of statistical

209   significance is used.

210

211   **Trends in bloom parameters**

212   We evaluated the time series changes in bloom parameters using Mann-Kendall non-parametric trend

213   analysis. We calculated Kendall's tau test for the significance (two-tailed test) of a monotonic time series

214   trend (Mann, 1945) for bloom start day, magnitude, intensity and duration of the dominant bloom. We

215   also calculated Theil-Sen slopes of trend, which is the median slope joining all pairs of observations. In

216   addition to absolute Theil-Sen slopes, we also calculated relative Theil-Sen slopes, where the slope is

217   joining each pair of observations divided by the first of the pair before the overall median is taken. Trend

218   tests and slope estimates were limited to grid locations with at least 10 detected blooms. Mean relative

219   Theil-Sen slopes were calculated over 5° latitude and longitude bands excluding data from latitudes

220   north and south of 62°N and 62°S, respectively. Absolute trends, calculated as the product of the

221   absolute Theil-Sen slope and the length of study period, were summarized on a global and regional

222   basis. In addition to the data requirements on number of blooms, outliers, as identified as estimates

223   outside the range of ±2 standard deviations of the mean, were removed. Global mean trends were

224   expressed by trend test probability intervals and cumulative intervals. While individual grid cells with

225   probabilities > 0.05 inevitably have a Theil-Sen slope whose 95% confidence interval overlaps with zero,

226   we nevertheless opted to examine all probability intervals in order to see if any global or regional

227   patterns emerged in the direction and magnitude of the mean Theil-Sen slopes when examined across

228   all grid cells. Probabilities were rounded to intervals of 0.1 such that interval 0.0 includes p<0.05,

7

229   interval 0.1 includes 0.05≤p<0.15, etc. The cumulative trends are based on the same data as the interval

230   trends summing data over each progressive probability interval. Regional trends were based on eight

231   subdivisions of the world ocean (see Fig. 1) and the contrast between oligotrophic and non-oligotrophic

232   ocean areas, eutrophic and mesotrophic areas (see: ocean.acri.fr/multicolore for source of oligotrophic

233   ocean mask). These regional trends were presented for probability interval 0.0 and cumulative interval

234   1.0 only.

235

236   **Effects of abiotic factors on bloom parameters**

237   We considered a suite of five abiotic factors that may be related to bloom timing and the size of blooms

238   through regionally varying mechanisms. Sea surface temperature (SST) extracted from the NOAA

239   Optimum Interpolation Sea Surface Temperature Analysis datasets (OISST), provides SST with a spatial

240   grid resolution of 1.0° and temporal resolution of 1 month (Reynolds *et al.*, 2002). The dataset uses *in*

241   *situ* data from ships and buoys as a means of adjusting for biases in satellite data. Salinity, mixed layer

242   depth (MLD), and zonal and meridional wind stress data were extracted from the Ocean Data

243   Assimilation Experiment, which incorporates near-real time data into an ocean model to estimate ocean

244   state parameters (Zhang *et al.*, 2007). The data are distributed on a non-standard global grid (360

245   longitudinal data points by 200 latitudinal data points) that was resampled to a 1.0° grid resolution and

246   temporal resolution of 1 month. Bloom parameters were correlated to the abiotic factors at monthly

247   (month and year of the bloom) and annual (mean of the year of the bloom) time resolutions for each

248   global grid location. We also calculated relative Theil-Sen slopes of abiotic factors and calculated mean

249   slopes over 5° latitude and longitude bands excluding data from latitudes north and south of 62°N and

250   62°S, respectively. These latitude and longitude means of the abiotic factors were correlated with the

251   matching latitude and longitude mean relative Theil-Sen slopes of bloom parameters.

252

253   **RESULTS**

254

255   **Dominant bloom characteristics**

256   The timing and size of the dominant bloom varied globally revealing distinct patterns often associated

257   with latitudinal bands. Bloom frequency had an interquartile range of 67% and 89% over the global

258   ocean (Fig. 2a), which may seem low considering we selected the detection time frame that produced

259   the most bloom detections. An algorithm optimized to find the maximum number of blooms may be

260   expected to detect a bloom in most years. It should be noted that while setting a constraint on bloom

8

261   duration was necessary to categorize a spatially and temporally variable phenomenon, this constraint

262   can result in 'missing' blooms. For instance, the bloom duration constraint may underestimate bloom

263   frequency in areas where the dominant bloom tends to be a multi-season event. This can be seen in the

264   North Atlantic frequency data where a segment of the Northeast Atlantic has relatively low bloom

265   frequency; detailed analysis of this region showed the blooms tended to be of long duration often

266   exceeding the duration constraint resulting in non-detection in some years (Friedland *et al.*, 2016). Most

267   of the eastern North Pacific has bloom frequency closer to the lower end of the interquartile range

268   contrasting the distinct latitudinal patterns found in the South Pacific. The South Atlantic and Indian

269   oceans were dominated by high bloom frequencies; however, the highest bloom frequencies at the

270   basin scale appear to be associated with the North Atlantic.

271   The mean start day of the dominant bloom was arrayed primarily by latitude. At high latitudes in

272   the southern hemisphere, the dominant bloom started near the end of the calendar year typically

273   having start days in the 300s, November-December (Fig. 2b). This coincides with austral spring.

274   Progressing equatorward, start day of blooms at lower latitudes in the southern hemisphere shifted to

275   earlier in the year over an approximate range of day 150 to 250 (June – August), which corresponds to

276   austral winter. North of the equator, there was a band of bloom start days at the end of the calendar

277   year with similar timing to the dominant bloom in the Antarctic. In the temperate Northern Hemisphere,

278   there was a band of spring blooms with start days ranging from approximately day 50-150 (March –

279   May), shifting to summer blooms in the high northern latitudes with start days in the 200s (June – July).

280   Thus, in both hemispheres, there are similar latitudinal patterns where fall/winter blooms are dominant

281   at low-to-mid latitudes and spring/summer blooms occur in subpolar and polar ecosystems.

282   Bloom magnitude was lowest in the oligotrophic ocean areas and highest in shelf seas and the

283   northern hemisphere. Over much of the north Atlantic and Pacific, bloom magnitude was between 10.0-

284   15.0 mg m^{-3} 8-day [1.0-1.2 log (mg m^{-3} 8-day +1); Fig. 2c]. For the areas of the globe between

285   approximately 40°N to 60°S, bloom magnitude was typically <5.0 mg m^{-3} 8-day [< 0.8 log (mg m^{-3} 8-

286   day+1)], with values in the oligotrophic ocean ranging from 0.5-1.5 mg m^{-3} 8-day [0.2-0.3 log (mg m^{-3} 8-

287   day+1)]. Bloom intensity followed a similar pattern to bloom magnitude with its lowest values in the

288   oligotrophic ocean and highest in shelf seas and the northern hemisphere (see Appendix S1). In the

289   northern hemisphere above 50°N, bloom intensity was approximately 2.0-4.0 mg m^{-3} [0.5-0.7 log (mg m^{-}

290   ^{3}+1)] and tended to be between 1.0-1.5 mg m^{-3} [0.3-0.4 log(mg m^{-3}+1)] over the latitude range of 40°N

291   to 60°S. Bloom intensity in the oligotrophic ocean was <0.2 mg m^{-3} [< 0.1 log (mg m^{-3}+1)] in many areas.

292   Mean bloom duration of the dominant bloom was longest in much of the oligotrophic ocean and

293   shortest in shelf seas and the higher latitude areas of the northern and southern hemispheres. Bloom

294   duration tended to exceed 60 days, or two months, in these oligotrophic ocean areas and was often as

295   short as one month in continental shelf ecosystems (Fig. 2d).

296

297   **Effect of bloom timing on bloom duration and size**

298   The timing of the dominant bloom was related to multiple measures of bloom size including bloom

299   duration, magnitude, and intensity. Over global scales, bloom timing was negatively correlated to bloom

300   duration, indicating that early blooms lasted longer than blooms that began later in the year (Fig. 3a).

301   Very few grid locations had significant positive correlations (~0.1%) indicative of early blooms of short

302   duration. Instead, fully half (50%) of the global grid was found to have significant negative relationships

303   between bloom start and duration.

304   The correlation between bloom start and magnitude was less robust (Fig. 3b), but reflected the

305   strong correlation found with duration. Over the global grid, most locations had non-significant

306   correlation between bloom start and magnitude (70%). For those locations with significant correlations,

307   98% had significant negative correlation indicating that early blooms produced high magnitude blooms.

308   The latter result was most likely related to the underlying correlation between bloom start and duration,

309   as duration is a key component in the calculation of magnitude; longer lasting blooms will likely have

310   higher magnitudes. Locations with significant negative correlations between bloom start and magnitude

311   tended to occur at mid-latitudes in both hemispheres.

312   The final relationship considered was between bloom timing and intensity. These data produced

313   the weakest correlation field with 82% of the global grid found to be non-significant. Of the significant

314   correlations, 92% were significant positive correlations indicating that later starting blooms were of

315   higher intensity or associated with higher mean [Chl] (Fig. 3c).

316

317   **Relative trends in bloom parameters**

318   The relative Theil-Sen slopes of the bloom parameters start day, magnitude, intensity, and duration

319   reveal distinct regional and global patterns. Distinct clusters of negative trends in bloom start day (i.e.,

320   earlier blooms) can be seen in the southern Pacific, Atlantic, and Indian oceans (Fig. 4a). Distinct clusters

321   of positive trends in bloom magnitude (i.e., increasing magnitude) and bloom intensity (i.e., increases in

322   intensity) can be seen across higher latitudes in both northern and southern hemispheres (Fig. 4b and

323   4c). Also negative trends in bloom magnitude and intensity were more common at low latitudes. While

10

324 present, trends in bloom duration were less spatially coherent making spatial patterns difficult to

325 identify (Fig. 4d).

326   Averaging relative Thiel-Sen slopes over latitude and longitude bins revealed distinct

327 distributional patterns. Mean relative Thiel-Sen slopes for bloom start day binned over latitude show

328 that slopes tended to be negative over most latitudes with the largest relative change found in the

329 southern hemisphere (Fig. 5a). Mean slopes for magnitude were positive at high latitudes and negative

330 for bands around the equator (Fig. 5c), with positive slopes increasing with latitude. Mean slopes for

331 intensity were arrayed by latitude in a similar fashion to magnitude (Fig. 5e). Mean relative Thiel-Sen

332 slopes for bloom duration tended to be positive over most latitudes with the exception of a group of five

333 high latitude northern bands that were negative indicating a shortening of blooms at these latitudes

334 (Fig. 5g). Mean relative Thiel-Sen slopes for bloom start day binned over longitude show that slopes

335 tended to be negative over most longitudes (Fig. 5b). Mean slopes for magnitude were positive for most

336 longitudes with the exception of a cluster associated with the Indian Ocean (Fig. 5d). Mean slopes for

337 intensity were arrayed by longitude in a similar fashion to magnitude (Fig. 5f). Mean relative Thiel-Sen

338 slopes for bloom duration tended to be positive over most longitudes with the exception of ranges of

339 longitudes associated with Indian and Atlantic oceans (Fig. 5h). Compared to other variables, fewer

340 slopes for bloom duration were significantly different from zero.

341

342 **Effects of abiotic factors on bloom parameters**

343 Our efforts to detect global scale relationships between abiotic factors and bloom characteristic yielded

344 mixed results. The correlation analysis examining the effect of abiotic factors including SST, salinity,

345 mixed layer depth, and wind stress did not reveal any comprehensive global relationships between

346 these factors and dominant bloom dynamics. The monthly and mean annual correlations are presented

347 in supporting information Appendix S2 (figures s2-1-10). These correlation fields are dominated by grid

348 locations with non-significant correlations. However, some inference on the effect of the abiotic factors

349 may be made by comparing their time series trend patterns to the patterns in time series trends in

350 bloom parameters.

351   Relative Thiel-Sen slopes of trends in SST suggest the most dramatic changes in thermal

352 conditions have occurred at high latitudes associated with changes in patterns of sea ice extent and

353 polar amplification of climate change, noting however that most of these data fall outside the latitude

354 constraints (>62° N/S) used here in most analyses (Fig. 6a). At lower latitudes, SST trends were generally

355 positive with the exception of the parts of the North Atlantic, the western North Pacific, and the eastern

356   South Pacific. Salinity has changed dramatically in isolated high latitude locations in the North Atlantic,

357   likely related to an increase in Arctic melting, where elsewhere over the global ocean there has been a

358   high degree of variability in salinity (Fig. 6b). Mixed layer depth trends have been mostly positive, and to

359   a higher degree in the southern hemisphere, although a lot of spatial variability in trends is evident in

360   the northern hemisphere (Fig. 6c). Both zonal and meridional wind stress have generally declined

361   globally, with a pattern of zonal wind decline most intense along certain lines of latitude (60° S, 30° S, 0°,

362   30° N, and 60° N) and meridional decline apparently circumscribing basin-scale oceanic gyres (Figs.

363   6d&e, respectively). Areas with the most intense declines in zonal wind stress correspond to the

364   transition zones between trade winds and westerly winds.

365   Trends in abiotic factors were summarized by latitude and longitude in the same manner as

366   bloom parameter trends were summarized in Figure 5. Mean relative Thiel-Sen slopes for SST binned

367   over latitude show that slopes tended to be positive over most latitudes with the largest relative

368   changes found at high latitudes, with a secondary peak just north of the equator (Fig. 7a). SST slopes

369   were also positive over most longitudes with the exception of bands associated with parts of the North

370   Atlantic, the western North Pacific, and the eastern South Pacific (Fig. 7b). SST was positively correlated

371   with bloom intensity and negatively correlated with bloom duration over latitudinal bins whereas it was

372   uncorrelated with bloom start and magnitude (Table 1). There were no significant correlations between

373   SST and bloom parameters arrayed by longitude. There did not appear to be a pattern in the latitudinal

374   distribution of salinity slopes; however, the longitudinal pattern suggests an anomalous freshening of

375   the Indian Ocean compared to other ocean areas (Figs. 7c & d, respectively). Despite weak latitudinal

376   patterns, salinity over latitude was correlated with latitudinal pattern of bloom intensity. The

377   longitudinal patterns of salinity trend were positively correlated with bloom magnitude and duration.

378   Slopes of mixed layer depth are mostly positive over latitudinal intervals, with the higher values at

379   higher latitudes; the only areas with negative slopes were associated with the lower latitudes of the

380   northern hemisphere (Fig. 7e). The increase in mixed layer depth appear highest in the Atlantic Ocean

381   basin compared to other areas based on longitudinal summary of slopes (Fig. 7f). Mixed layer depth

382   trend over latitude was uncorrelated with bloom parameters, but were positively correlated with all

383   four bloom parameter over longitudinal bins. Mean slopes were almost all negative for zonal wind

384   stress, over latitude and longitude, with little evidence of spatial patterns in either data summary (Figs.

385   7g & h, respectively). The only significant correlation between zonal wind stress and bloom parameter

386   was found with bloom duration over longitude. Likewise, mean meridional wind stresses were almost all

387   negative over latitudes and longitudes; however, there may be some level of patterning in the latitudinal

388 distribution of mean slopes with the largest change occurring at middle latitudes (Figs. 7i & j,

389 respectively). These changes in meridional wind stress over latitude were negatively correlated with

390 bloom magnitude and intensity. Longitudinal patterns of meridional wind stress trends was negatively

391 correlated with bloom start.

392

393 **Mean Absolute Trends in bloom parameters**

394 Absolute trends expressed as change in bloom parameters over the study period suggest there have

395 been substantial shifts in bloom timing and size. Bloom start day has shifted on the order of 3 days

396 earlier on a global basis and for regions associated with statistically significant shifts, blooms have

397 advanced on the order of two weeks (Fig. 8a). Bloom magnitude and intensity have both increased on a

398 global basis on the order of 0.3 mg m^{-3} 8-day and 0.05 mg m^{-3}, respectively, which represents about a

399 10% increase in both parameters (Fig. 8b&c). The increases in these parameters in regions associated

400 with statistically significant shifts have been much greater and on the order of 0.9 mg m^{-3} 8-day and 0.4

401 mg m^{-3}, respectively, which represents about a 35% increase again for both. Bloom duration has shifted

402 on the order of 2 days longer on a global basis and for regions associated with statistically significant

403 shifts, blooms have lengthened on the order of one week (Fig. 8d).

404   The bloom absolute trends partitioned by the eight subdivisions of the world ocean and the

405 between oligotrophic and non-oligotrophic ocean areas differed from the global means in a number of

406 ways. Bloom start had negative trends, indicating earlier blooms, in all ocean areas; but, the trend was

407 greater in the southern oceans and in oligotrophic areas (Fig. 9a). For regions associated with

408 statistically significant shifts, the North Atlantic had a positive bloom start trend suggesting that the

409 bloom started approximately five days later, whereas the other ocean areas had negative trends

410 suggesting shifts of 1-3 weeks (Fig. 10a). Bloom magnitude and intensity had positive trends in the

411 northern and southern oceans and between oligotrophic and non-oligotrophic regions (Fig. 9b&c). The

412 tropical ocean areas either had zero or negative trends in these parameters. The pattern of change in

413 magnitude and intensity in the regions associated with statistically significant shifts were nearly identical

414 to the global averages, but the size of the shifts was larger when considering only statistically significant

415 results (Fig. 10b&c). Bloom duration increased in all areas except the North Atlantic and tropical Indian

416 oceans where the trend confidence interval included zero (Fig. 10d). The pattern of change in duration

417 in the regions associated with statistically significant shifts was similar to the global patterns; however,

418 four regions had confidence intervals that included zeros (Fig. 10d).

419

DISCUSSION

Our analysis of phytoplankton blooms on a global scale suggests directional time series change in the timing, duration, and size of blooms, which portends changes in the functioning of marine ecosystems and carbon cycling from local to basin scales (Ji *et al.*, 2010). Notably, we provide evidence that blooms are initiating earlier in the year, having shifted in timing on the order of weeks in some regions, and are of longer duration suggesting the timing of bloom cessation has also changed. There have also been changes in the pattern of bloom size, suggesting an increase in bloom size at high latitudes and a decrease at low latitudes in a gradated fashion. It is critical to understand these changes in bloom dynamics since they provide labile biomass that form the basis of food webs and are fundamentally important to the biogeochemical functioning of marine ecosystems (Sigman & Hain, 2012).

The low spatial coherence between correlations of the abiotic factors and bloom intensity and magnitude is in stark contrast to the high spatial coherence of global trends in these bloom parameters and time series trends in the abiotic factors, suggesting the importance of variability and local factors in the control of blooms on a global scale. Local changes in salinity and temperature affect stratification, which can trap phytoplankton above the pycnocline and decrease nutrient inputs from deeper layers, while decreased wind-driven mixing will exacerbate this scenario. In a global comparison of the effects of stratification on chlorophyll biomass, Dave and Lozier (2013) showed mixed trends in stratification over much of the globe, with much of the eastern subtropical Pacific experiencing increased stratification, while much of the Atlantic experiencing decreased stratification. However these changes were not well correlated with trends in chlorophyll concentrations, further suggesting the importance of local processes controlling blooms. Similar to the results presented in this study, Dave and Lozier (2013) found trends in decreasing stratification over much of the mid- and lower latitudes, which were driven primarily by increased rates of warming of subsurface water relative to surface waters, resulting in an increased mixed layer depth.

Though clearly not a test of hypotheses, the comparison of latitudinal and longitudinal patterns of trends in potential abiotic forcing factors may offer some insights on both global and regional changes in bloom dynamics. The latitudinal patterns in SST and meridional wind stress trends are similar to the latitudinal pattern in bloom duration in that all show bimodal distributions at low latitudes. This particular pattern is consistent with an increase in bloom duration in the Baltic Sea that also coincided with warming temperatures and decreased winds (Groetsch *et al.*, 2016). Likewise, there are features in the latitudinal pattern of mixed layer depth that match the latitudinal patterns in bloom magnitude and intensity trends. Furthermore, the advance in bloom timing over all latitudes may be related to the

14

452   global changes in wind stress. The most striking longitudinal pattern in global bloom dynamics is

453   associated with the Indian Ocean characterized by reductions in bloom magnitude, intensity, and

454   duration corresponding roughly with meridians 50° to 100° E. Phytoplankton dynamics in the Indian

455   Ocean have been considered in the context of abiotic forcing. Goes *et al*. (2005) and Gregg *et al*. (2005)

456   documented increases in net primary production in the western Indian Ocean; however, a more recent

457   study is consistent with our findings, suggesting a reduction in [Chl] over the past 16 years (Roxy *et al.*,

458   2016). These researchers attributed the change in [Chl] to a reduction in available nutrients in the

459   euphotic zone due to increasing SST that increased stratification-induced trapping of nutrients in the

460   deeper Indian Ocean. The confounding influence of increasing SST trends on mixing and phytoplankton

461   growth rates make prediction of phytoplankton dynamics difficult, especially in the Indian Ocean, an

462   area experiencing the largest warming trend in the tropical ocean (Roxy *et al.*, 2014). However, it is

463   worth noting that the most striking longitudinal pattern in the abiotic data we found was in the salinity

464   data suggesting a freshening of Indian Ocean waters, which may have amplified thermal effects on

465   stratification as described due to changes in monsoon patterns.

466   A general decrease in zonal and meridional wind stress has the potential to impact production

467   by reducing the wind-driven mixing in areas of light-limited production (Kim *et al.*, 2007). Contrary to

468   this, while our analysis suggests an overall decrease in winds on a broad scale, there is an associated

469   broad increase in the mixed layer depth. This may be due in part to local changes in temperature and

470   salinity affecting stratification. While most regions of the globe are experiencing decreasing wind stress,

471   the few regions where wind stress is increasing are also experiencing the largest increases in mixed layer

472   depth, such as in the southern Atlantic Ocean at 60°S. This is likely a result of higher mean wind speeds

473   in these locations since the power of wind exerted on the water scales with the cube of mean wind

474   speed. Therefore, even a small increase in wind stress in an area can result in profound changes in wind-

475   driven mixing and increased MLD. The global trends in MLD bear a striking resemblance to the global

476   trends in bloom intensity, and to a lesser degree, bloom magnitude. However, the spatial correlations

477   between MLD and these bloom parameters is low and bears few spatially significant regions, save for

478   the oligotrophic southern subtropical Pacific, where enhanced mixing may enhance nutrient

479   concentrations (de Boyer Montegut *et al.*, 2004). In the subpolar and northern subtropical regions of the

480   North Atlantic, Ueyama and Monger (2005) found an inverse relationship between bloom intensity and

481   wind-induced mixing, where decreased mixing during blooms resulted in enhanced bloom intensity,

482   while the opposite was true for the southern subtropical region where nutrients may be limiting

483   production and light penetration is greater. Atmospheric-related variability in wind-driven mixing was

484   also found to affect the timing of bloom initiation, where the start day of blooms in the North Atlantic

485   was strongly associated with the winter North Atlantic Oscillation index (Ueyama & Monger, 2005). A

486   similar relationship between wind speed and bloom timing has also been detected in the Japan Sea

487   (Yamada & Ishizaka, 2006). Furthermore, Moore *et al.* (2013), in a review of nutrient limitation dynamics

488   in the global ocean, concluded that nitrogen was limiting in much of the surface waters in tropical

489   latitudes, consistent with our observations. In areas where nitrogen is not limiting, iron limitation tends

490   to dominate (e.g., the Southern Ocean and the eastern equatorial Pacific (Behrenfeld *et al.*, 1996)). Iron

491   limitation may play a particularly large role in the differences we observed between the bloom dynamics

492   in the eastern North and South Pacific (Behrenfeld & Kolber, 1999).

493   Despite methodological differences in bloom detections and analyses, our results do align with

494   those from other global and basin-scale estimates of bloom parameters. Different bloom detection

495   algorithms lead to varying accuracy and precision of bloom phenology metrics (Ferreira *et al.*, 2014); and

496   consequently, varying depictions of bloom dynamics (Brody *et al.*, 2013). Our focus is on the dominant

497   annual bloom occurring within a grid cell and on the main period of elevated bloom conditions

498   constrained by the length of our detection time window. As a number of investigators have

499   characterized (Sapiano *et al.*, 2012; Taboada & Anadon, 2014), most areas of the globe are dominated

500   by a single bloom with the exception of some regions that are characterized by a secondary bloom in

501   regions predominately oriented in specific latitudinal bands. Despite this methodological difference, our

502   characterization of bloom start is similarly patterned to previous global (Racault *et al.*, 2012; Sapiano *et*

503   *al.*, 2012) and basin scale studies (Henson *et al.*, 2009; Taboada & Anadon, 2014; Zhang *et al.*, 2017).

504   However, our estimates of bloom duration are at variance with most studies owing to the contrast in

505   methods applied between studies. In studies estimating bloom duration using a threshold approach

506   (Siegel *et al.*, 2002), bloom duration tended to be 2-fold longer than ours (Racault *et al.*, 2012; Sapiano

507   *et al.*, 2012). However, the spatial patterns of long versus short bloom duration were consistent with our

508   results. The measures of bloom size, here referred to as magnitude and intensity and variously named

509   and applied by different investigators, were also similar between studies and generally followed

510   climatological patterns of the distribution of [Chl] (Doney *et al.*, 2003).

511   On a global scale, the spatial organization of areas with homogenous bloom dynamics appears

512   to have a high degree of zonal band patterning and more complex organization associated with

513   meridional bands (Sapiano *et al.*, 2012). For example, mean relative Thiel-Sen slopes for bloom duration

514   tended to be positive over most latitudes with exception of a group of five high latitude northern bands,

515   which were negative indicating a shortening of blooms at these latitudes. Mean slopes for magnitude

16

516   and intensity were positive for most longitudes with the exception of a cluster associated with the

517   Indian Ocean.

518   Changes in bloom timing and size were not uniform over the globe. Owing to contrasts in

519   oceanographically defined functional regions and latitudinal patterns, changes in bloom dynamics will

520   likely have different regional impacts. An analysis of spring and fall blooms in the north Atlantic and

521   Pacific basins that employed a spectral decomposition approach for bloom detection characterized

522   regional scale time series change in bloom timing and magnitude (equivalent to bloom intensity as used

523   here) that hold many similarities to the patterns described in our analysis (Zhang *et al.*, 2017). Bloom

524   timing was alternatively advanced and delayed on the order of weeks with coherent trends in matching

525   areas of both basins. It is difficult to compare our trends in bloom intensity to their results for trends in

526   magnitude since our spatial characterization is based on relative Theil-Sen slopes. Similarly, in a study

527   focused on the North Atlantic, Taboada and Anadon (2014) provided estimates of bloom intensity trends

528   that match our study results; however, their method of estimating bloom timing trends differed from

529   those presented here. Racault *et al.* (2012) estimated trends in bloom duration on a global scale also

530   using linear regression, but with a time series restricted to the length of the SeaWiFS time series only

531   (1998-2007). Their estimates of global trends in bloom duration were mostly negative indicating a

532   tendency for blooms to be shortened over global scales. We note, however, that their time series is

533   shorter than that analyzed here and bloom duration was estimated using a threshold approach (Siegel *et*

534   *al.*, 2002), which, as noted above, provides estimates of bloom duration 2-fold longer than ours. Hence,

535   they are estimating a different aspect of phytoplankton dynamics, whereas we are focusing on the

536   discrete portion of the bloom associated with highly elevated [Chl].

537   We view our results in the context of changes that have occurred and will likely occur to the

538   global climate system. Global thermal conditions are changing and it is important to consider change in

539   the level of system variability and its impact on ecosystems (Vazquez *et al.*, 2017). Change in thermal

540   regime is having profound effects on atmospheric circulation and the forcing factors related to bloom

541   development, which may be more important to phytoplankton than the direct effect of change in

542   thermal regime itself (Francis & Vavrus, 2015). The latitudinal changes in bloom magnitude and intensity

543   are also consistent with the effects of global thermal change on phytoplankton community composition

544   (Marinov *et al.*, 2010), shifting communities to include members which are capable of different growth

545   rates or resistance to grazing that allow for a change in [Chl]. Furthermore, changing thermal regimes

546   have been associated with shifting species composition of blooms, where for a fixed study site blooms

547   have become increasingly dominated by the genus *Synechococcus* (Hunter-Cevera *et al.*, 2016). The

17

548 changing role of cyanobacteria is expected to have a profound effect on plankton dynamics in a range of

549 aquatic systems (Visser *et al.*, 2016). We can also expect changes to the seasonal nature of blooms

550 (Henson *et al.*, 2013) and likely impacts on secondary production as well (Litchman *et al.*, 2006). The

551 change in dominant bloom timing we observed is consistent with the effect of an increase in global

552 temperature and its role in mixed layer dynamics, though the rate of stratification and turbulent mixing

553 remains unclear (Franks, 2015). These are changes to the base of food web warrant further

554 investigation.

555 　　　　Change in phytoplankton bloom dynamics would be expected to impact the rate of flux of

556 particulate organic carbon (POC) from the water column to the benthos. Parts of the world ocean are

557 dominated by production cycles that are characterized by blooms associated with high concentrations of

558 biomass whereas other regions have bloom features that are not as prominent, though in many cases

559 primary production can still be at a high level (Reygondeau *et al.*, 2013). However, phytoplankton

560 blooms, in particular, support conditions that result in the intense flux of POC (Reigstad *et al.*, 2011;

561 Belley *et al.*, 2016). It follows that changes in the timing and size of a bloom will affect the amount of

562 POC exported to the benthos. Over most regions of the globe, blooms appear to have lasted longer,

563 which could result in an increase in POC flux. Bloom magnitude and intensity have changed over

564 latitudinal ranges, most notably with decreased bloom magnitude at low latitude and increases at high

565 latitudes. Similar changes in bloom magnitude across a range of latitudes were obtained in a study that

566 used an earth system model that included data assimilation to examine changes in North Pacific bloom

567 characteristics since the 1960s (Asch, 2013). Together these results indicate that POC fluxes to the

568 benthos may increase at high latitudes, while decreasing at lower latitudes. These changes in bloom

569 dynamics should be taken into account in global carbon flux estimation models.

570 　　　　Species composition of phytoplankton communities varies over global scales and is principally

571 influenced by dispersion and competitive exclusion (Barton *et al.*, 2010). However, species composition

572 is also influenced by environmental conditions, such as mixing regimes and light conditions, (Barton *et*

573 *al.*, 2015) leading to concerns that shifting thermal conditions will actuate shifts to smaller size taxa

574 (Moran *et al.*, 2010). These smaller producers have different dynamics and vertical transport properties,

575 which have the potential to affect both export flux and the way an ecosystem functions (Mouw *et al.*,

576 2016). Utilizing phytoplankton size estimated from remote sensing data (Kostadinov *et al.*, 2016; Mouw

577 *et al.*, 2017), Mouw *et al.* (2016) contrasted the difference in export flux and transfer efficiency during

578 times dominated by small and large cells within biogeochemical provinces. They found periods

579 dominated by small cells to have both greater export flux efficiency and lower transfer efficiency than

580   periods dominated by large cells. Rising temperatures will likely shift phytoplankton niches poleward

581   and are predicted to have the greatest potential impact on tropical phytoplankton diversity (Thomas *et*

582   *al.*, 2012). Considering the importance of species groups to the role of phytoplankton production, the

583   phenology of various methods to determine phytoplankton size has been compared (Kostadinov *et al.*,

584   2017) and the phenology of some methods has been connected to environmental conditions (Cabré *et*

585   *al.*, 2016; Soppa *et al.*, 2016). However, the changes in phenology of various phytoplankton groups have

586   yet to be explored, which could provide refinements to both retrospective and forecasted modelling

587   efforts.

588   This study provides substantial evidence to support the observation that early blooms are longer

589   lasting blooms and conversely delayed bloom start is associated with shorter blooms. This phenomenon

590   has been described previously on a global scale (Racault *et al.*, 2012) and for the North Atlantic

591   (Friedland *et al.*, 2016), with the latter study exploring the hypothesis that bloom duration is in large

592   measure shaped by grazing by zooplankton that have a diapause life cycle. It is important to note that

593   despite using a different bloom measurement methodology, results from Racault *et al*. (2012) and for

594   the North Atlantic (Friedland *et al.*, 2016) agree with the current study in the overall nature of the

595   relationship (i.e., the direction of trends and coherence at large spatial scales), but differ in the fine scale

596   regional patterning of this correlation. It may be through this regional patterning that we are able to

597   evaluate the relative role of nutrient limitation and grazing in shaping bloom development (Evans &

598   Parslow, 1985; Fasham *et al.*, 1990). The latitudinal banding of this relationship would have to be

599   reflected in the nature of pre-bloom mixing and initial nutrient supply over a range of physical

600   environments for nutrient supply to be the unifying factor controlling bloom duration as a function of

601   bloom initiation. This work has yet to be done, but in a practical sense has a better chance of being

602   accomplished considering the paucity of grazing information in most parts of the world ocean.

603   The observational results of this study provide some level of validation for earth systems models

604   that simulate global climate and ocean systems dynamics. Multiple earth system models suggest that

605   climate change will have the greatest impact on bloom phenology at high latitudes (Henson *et al.*, 2013).

606   Under a business-as-usual emissions scenario, the month of maximum primary productivity is projected

607   to advance by 0.5-1 months by the end of the 21st century across many ocean ecosystems. The

608   exception to this pattern is the oligotrophic subtropical gyres where delays in the timing of peak primary

609   production have been projected. These changes have been attributed to earlier easing of light limitation

610   due to increases in stratification (Henson *et al.*, 2013). These future projections utilize earth system

611   model outputs with a monthly resolution, so additional research that can detect finer scale changes in

612 phenology is needed. One study that used finer temporal resolution data from the NCAR Community

613 Earth System Model (CESM) model assimilated historical data on atmospheric observations and sea

614 surface temperature (Asch, 2013). In contrast to models of future projections, this study of historical

615 patterns identified the largest trends in bloom phenology in oligotrophic areas (Asch, 2013), which may

616 reflect an influence of inter-annual climate variability rather than climate change. Our observational

617 results are consistent with this pattern, and thus provide an indication of the skill of the NCAR model,

618 which did not assimilate any ocean color data.

619 As ocean color time series have grown in length, there have been efforts to describe time series

620 trends in bloom characteristics. Importantly, these efforts have included disciplined analyses of the

621 requirements to detect trends in the face of noisy and incomplete data and whether trends can be

622 attributed to climate change or not (Beaulieu *et al.*, 2013; Henson *et al.*, 2016). Furthermore, Henson *et*

623 *al.* (2013) estimates that it would require ~ 30 years of data to distinguish trends in bloom phenology

624 from natural decadal variability. Given the results of these investigations, we approach our findings with

625 caution. As encouraging as it is to now have a nearly twenty-year time series of data, it is difficult to be

626 conclusive about the description of trends and to attribute any of these trends to climate change.

627 However, it is reasonable to compare these trends to observed climate variation over the past two

628 decades and discuss whether these trends are consistent with future projections under different climate

629 change scenarios.

630

631 **CONCLUSIONS**

632 The timing and size of phytoplankton blooms have changed on both regional and global scales. This

633 finding is important because blooms play a pivotal role in the flow of energy in marine ecosystems,

634 impacting the way food webs work and the way these ecosystems provide a range of services. The

635 dominant bloom was found to vary with latitude and in localized patterns associated with specific

636 oceanographic features. Blooms have increased in magnitude and intensity at high latitudes and

637 decreased in equatorial areas. Overall, blooms started earlier and lasted longer, with bloom timing

638 having the most profound effect on bloom duration; early blooms tended to last longer than later

639 starting blooms. This finding has the potential to impact phenological relationships between producer

640 and consumer species such as mesozooplankton and higher trophic position fish and invertebrates.

641 Timing mechanisms for reproduction in many species have evolved that ensure adequate forage for

642 early life stages, which may be impacted by changes in bloom timing. In regions where blooms last

643 longer and are associated with higher [Chl], the dynamics of the biological pump are likely to alter the

644 rates of carbon cycling and export. A shift to earlier bloom timing is consistent with the expected effect

645 of warming ocean conditions seen in recent decades. It is incumbent upon assessment and modelling

646 practitioners to account for the dynamic variability of phytoplankton production.

647

648

654

655 **Data Accessibility Statement**

656

657 All chlorophyll concentration data is available as NCDF files from the GlobColour products databased

658 located at: http://hermes.acri.fr/?class=archive. Ocean Data Assimilation Experiment data is located at:

659 https://www.gfdl.noaa.gov/ocean-data-assimilation.

660

661

662 **Biosketch**

663

664 Kevin Friedland is a researcher with the National Marine Fisheries Service at the Narragansett

665 Laboratory in Rhode Island, USA. He holds a bachelors degree in ecology from Rutgers College in New

666 Jersey and a doctorate from the College of William and Mary in Virginia. His dissertation research was

667 on the distribution and feeding ecology of Atlantic menhaden. During his professional career, he has

668 done research on menhaden, bluefish, sea herring, sturgeon, eel, cod, haddock, and salmon. His

669 publications cover a range of topics including: estuarine ecology of fishes, functional morphology,

670 feeding ecology, recruitment processes, fisheries oceanography, stock identification, ecosystem ecology,

671 and climate change. His current research is on the effects of bloom phenology on ecosystem function.

672 He has served as the chair of several International Council for the Exploration of the Sea (ICES) scientific

673 working groups and is currently the US representative to SCICOM.

674

675

676 **REFERENCES**

677

678 Asch, R.G. (2013) Interannual-to-Decadal Changes in Phytoplankton Phenology, Fish Spawning Habitat,
679   and Larval Fish Phenology. *Ph.D. dissertation, University of California, San Diego. 268 p.*,

680   Barton, A.D., Lozier, M.S. & Williams, R.G. (2015) Physical controls of variability in North Atlantic
681   phytoplankton communities. *Limnology and Oceanography*, **60**, 181-197.
682   Barton, A.D., Dutkiewicz, S., Flierl, G., Bragg, J. & Follows, M.J. (2010) Patterns of diversity in marine
683   phytoplankton. *Science*, **327**, 1509-1511.
684   Beaulieu, C., Henson, S.A., Sarmiento, J.L., Dunne, J.P., Doney, S.C., Rykaczewski, R.R. & Bopp, L. (2013)
685   Factors challenging our ability to detect long-term trends in ocean chlorophyll. *Biogeosciences*,
686   **10**, 2711-2724.
687   Behrenfeld, M.J. & Kolber, Z.S. (1999) Widespread iron limitation of phytoplankton in the South Pacific
688   Ocean. *Science*, **283**, 840-843.
689   Behrenfeld, M.J. & Boss, E.S. (2014) Resurrecting the ecological underpinnings of ocean plankton
690   blooms. *Annual Review of Marine Science, Vol 6, 2014*, **6**, 167-U208.
691   Behrenfeld, M.J., Bale, A.J., Kolber, Z.S., Aiken, J. & Falkowski, P.G. (1996) Confirmation of iron limitation
692   of phytoplankton photosynthesis in the equatorial Pacific Ocean. *Nature*, **383**, 508-511.
693   Belley, R., Snelgrove, P.V.R., Archambault, P. & Juniper, S.K. (2016) Environmental drivers of benthic flux
694   variation and ecosystem functioning in Salish Sea and Northeast Pacific sediments. *Plos One*, **11**
695   Blondeau-Patissier, D., Gower, J.F.R., Dekker, A.G., Phinn, S.R. & Brando, V.E. (2014) A review of ocean
696   color remote sensing methods and statistical techniques for the detection, mapping and analysis
697   of phytoplankton blooms in coastal and open oceans. *Progress in Oceanography*, **123**, 123-144.
698   Brody, S.R., Lozier, M.S. & Dunne, J.P. (2013) A comparison of methods to determine phytoplankton
699   bloom initiation. *Journal of Geophysical Research-Oceans*, **118**, 2345-2357.
700   Cabré, A., Shields, D., Marinov, I. & Kostadinov, T.S. (2016) Phenology of size-partitioned phytoplankton
701   carbon-biomass from ocean color remote sensing and CMIP5 models. *Front. Mar. Sci.*, **3**, 591–
702   20.
703   Chassot, E., Bonhommeau, S., Dulvy, N.K., Melin, F., Watson, R., Gascuel, D. & Le Pape, O. (2010) Global
704   marine primary production constrains fisheries catches. *Ecology Letters*, **13**, 495-505.
705   Cherkasheva, A., Bracher, A., Melsheimer, C., Koberle, C., Gerdes, R., Nothig, E.M., Bauerfeind, E. &
706   Boetius, A. (2014) Influence of the physical environment on polar phytoplankton blooms: A case
707   study in the Fram Strait. *Journal of Marine Systems*, **132**, 196-207.
708   Christensen, V., Coll, M., Buszowski, J., Cheung, W.W.L., Frolicher, T., Steenbeek, J., Stock, C.A., Watson,
709   R.A. & Walters, C.J. (2015) The global ocean is an ecosystem: simulating marine life and
710   fisheries. *Global Ecology and Biogeography*, **24**, 507-517.
711   Cole, H., Henson, S., Martin, A. & Yool, A. (2012) Mind the gap: The impact of missing data on the
712   calculation of phytoplankton phenology metrics. *Journal of Geophysical Research-Oceans*, **117**
713   Corbiere, A., Metzl, N., Reverdin, G., Brunet, C. & Takahashi, A. (2007) Interannual and decadal
714   variability of the oceanic carbon sink in the North Atlantic subpolar gyre. *Tellus Series B-*
715   *Chemical and Physical Meteorology*, **59**, 168-178.
716   Cushing, D.H. (1990) Plankton production and year-class strength in fish populations - an update of the
717   match mismatch hypothesis. *Advances in Marine Biology*, **26**, 249-293.
718   D'Ortenzio, F., Antoine, D., Martinez, E. & d'Alcala, M.R. (2012) Phenological changes of oceanic
719   phytoplankton in the 1980s and 2000s as revealed by remotely sensed ocean-color
720   observations. *Global Biogeochemical Cycles*, **26**
721   Dave, A.C. & Lozier, M.S. (2013) Examining the global record of interannual variability in stratification
722   and marine productivity in the low-latitude and mid-latitude ocean. *Journal of Geophysical*
723   *Research-Oceans*, **118**, 3114-3127.
724   Davison, P.C., Checkley, D.M., Koslow, J.A. & Barlow, J. (2013) Carbon export mediated by mesopelagic
725   fishes in the northeast Pacific Ocean. *Progress in Oceanography*, **116**, 14-30.

726 de Boyer Montegut, C., Madec, G., Fischer, A.S., Lazar, A. & Iudicone, D. (2004) Mixed layer depth over
727   the global ocean: An examination of profile data and a profile-based climatology. *Journal of*
728   *Geophysical Research-Oceans*, **109**

729 Doney, S.C., Bopp, L. & Long, M.C. (2014) Historical and future trends in ocean climate and
730   biogeochemistry. *Oceanography*, **27**, 108-119.

731 Doney, S.C., Glover, D.M., McCue, S.J. & Fuentes, M. (2003) Mesoscale variability of Sea-viewing Wide
732   Field-of-view Sensor(SeaWiFS) satellite ocean color: Global patterns and spatial scales. *Journal*
733   *of Geophysical Research-Oceans*, **108**

734 Evans, G.T. & Parslow, J.S. (1985) A model of annual plankton cycles. *Biol. Oceanogr.*, **3**, 327–347.

735 Fasham, M.J.R., Ducklow, H.W. & Mckelvie, S.M. (1990) A nitrogen-based model of plankton dynamics in
736   the oceanic mixed layer. *Journal of Marine Research*, **48**, 591-639.

737 Ferreira, A.S., Visser, A.W., MacKenzie, B.R. & Payne, M.R. (2014) Accuracy and precision in the
738   calculation of phenology metrics. *Journal of Geophysical Research-Oceans*, **119**, 8438-8453.

739 Ferreira, A.S.A., Hatun, H., Counillon, F., Payne, M.R. & Visser, A.W. (2015) Synoptic-scale analysis of
740   mechanisms driving surface chlorophyll dynamics in the North Atlantic. *Biogeosciences*, **12**,
741   3641-3653.

742 Field, C.B., Behrenfeld, M.J., Randerson, J.T. & Falkowski, P. (1998) Primary production of the biosphere:
743   Integrating terrestrial and oceanic components. *Science*, **281**, 237-240.

744 Francis, J.A. & Vavrus, S.J. (2015) Evidence for a wavier jet stream in response to rapid Arctic warming.
745   *Environmental Research Letters*, **10**

746 Franks, P.J.S. (2015) Has Sverdrup's critical depth hypothesis been tested? Mixed layers vs. turbulent
747   layers. *Ices Journal of Marine Science*, **72**, 1897-1907.

748 Frenken, T., Velthuis, M., Domis, L.N.D., Stephan, S., Aben, R., Kosten, S., van Donk, E. & Van de Waal,
749   D.B. (2016) Warming accelerates termination of a phytoplankton spring bloom by fungal
750   parasites. *Global Change Biology*, **22**, 299-309.

751 Friedland, K.D. & Todd, C.D. (2012) Changes in Northwest Atlantic Arctic and Subarctic conditions and
752   the growth response of Atlantic salmon. *Polar Biology*, **35**, 593-609.

753 Friedland, K.D., Hare, J.A., Wood, G.B., Col, L.A., Buckley, L.J., Mountain, D.G., Kane, J., Brodziak, J.,
754   Lough, R.G. & Pilskaln, C.H. (2008) Does the fall phytoplankton bloom control recruitment of
755   Georges Bank haddock, *Melanogrammus aeglefinus*, through parental condition? *Canadian*
756   *Journal of Fisheries and Aquatic Sciences*, **65**, 1076-1086.

757 Friedland, K.D., Leaf, R.T., Kane, J., Tommasi, D., Asch, R.G., Rebuck, N., Ji, R., Large, S.I., Stock, C. & Saba,
758   V.S. (2015) Spring bloom dynamics and zooplankton biomass response on the US Northeast
759   Continental Shelf. *Continental Shelf Research*, **102**, 47-61.

760 Friedland, K.D., Record, N.R., Asch, R.G., Kristiansen, T., Saba, V.S., Drinkwater, K.F., Henson, S., Leaf,
761   R.T., Morse, R.E., Johns, D.G., Large, S.I., Hjøllo, S.S., Nye, J.A., Alexander, M.A. & Ji, R. (2016)
762   Seasonal phytoplankton blooms in the North Atlantic linked to the overwintering strategies of
763   copepods. *Elementa*, **DOI: http://doi.org/10.12952/journal.elementa.000099**, p.99.

764 Goes, J.I., Thoppil, P.G., Gomes, H.D. & Fasullo, J.T. (2005) Warming of the Eurasian landmass is making
765   the Arabian Sea more productive. *Science*, **308**, 545-547.

766 Gregg, W.W., Casey, N.W. & McClain, C.R. (2005) Recent trends in global ocean chlorophyll. *Geophysical*
767   *Research Letters*, **32**

768 Groetsch, P.M.M., Simis, S.G.H., Eleveld, M.A. & Peters, S.W.M. (2016) Spring blooms in the Baltic Sea
769   have weakened but lengthened from 2000 to 2014. *Biogeosciences*, **13**, 4959-4973.

770 Henson, S., Cole, H., Beaulieu, C. & Yool, A. (2013) The impact of global warming on seasonality of ocean
771   primary production. *Biogeosciences*, **10**, 4357-4369.

772 Henson, S.A., Dunne, J.P. & Sarmiento, J.L. (2009) Decadal variability in North Atlantic phytoplankton
773   blooms. *Journal of Geophysical Research-Oceans*, **114 Doi 10.1029/2008jc005139**

Henson, S.A., Beaulieu, C. & Lampitt, R. (2016) Observing climate change trends in ocean biogeochemistry: when and where. *Global Change Biology*, **22**, 1561-1571.

Holt, J., Schrum, C., Cannaby, H., Daewel, U., Allen, I., Artioli, Y., Bopp, L., Butenschon, M., Fach, B.A., Harle, J., Pushpadas, D., Salihoglu, B. & Wakelin, S. (2016) Potential impacts of climate change on the primary production of regional seas: A comparative analysis of five European seas. *Progress in Oceanography*, **140**, 91-115.

Hunt, G.L., Stabeno, P., Walters, G., Sinclair, E., Brodeur, R.D., Napp, J.M. & Bond, N.A. (2002) Climate change and control of the southeastern Bering Sea pelagic ecosystem. *Deep-Sea Research Part Ii-Topical Studies in Oceanography*, **49**, 5821-5853.

Hunter-Cevera, K.R., Neubert, M.G., Olson, R.J., Solow, A.R., Shalapyonok, A. & Sosik, H.M. (2016) Physiological and ecological drivers of early spring blooms of a coastal phytoplankter. *Science*, **354**, 326-329.

Irigoien, X., Klevjer, T.A., Rostad, A., Martinez, U., Boyra, G., Acuna, J.L., Bode, A., Echevarria, F., Gonzalez-Gordillo, J.I., Hernandez-Leon, S., Agusti, S., Aksnes, D.L., Duarte, C.M. & Kaartvedt, S. (2014) Large mesopelagic fishes biomass and trophic efficiency in the open ocean. *Nature Communications*, **5**

Ji, R.B., Edwards, M., Mackas, D.L., Runge, J.A. & Thomas, A.C. (2010) Marine plankton phenology and life history in a changing climate: current research and future directions. *Journal of Plankton Research*, **32**, 1355-1368.

Kahru, M., Brotas, V., Manzano-Sarabia, M. & Mitchell, B.G. (2011) Are phytoplankton blooms occurring earlier in the Arctic? *Global Change Biology*, **17**, 1733-1739.

Kim, H.C., Yoo, S.J. & Oh, I.S. (2007) Relationship between phytoplankton bloom and wind stress in the sub-polar frontal area of the Japan/East Sea. *Journal of Marine Systems*, **67**, 205-216.

Kostadinov, T.S., Milutinovic, S., Marinov, I. & Cabre, A. (2016) Carbon-based phytoplankton size classes retrieved via ocean color estimates of the particle size distribution. *Ocean Science*, **12**, 561-575.

Kostadinov, T.S., Cabré, A., Vedantham, H., Marinov, I., Bracher, A., Brewin, R.J.W., Bricaud, A., Hirata, T., Hirawake, T., Hardman-Mountford, N.J., Mouw, C., Roy, S. & Uitz, J. (2017) Inter-comparison of phytoplankton functional type phenology metrics derived from ocean color algorithms and Earth System Models. *Remote Sensing of Environment*, **190**, 162-177.

Laufkotter, C., Vogt, M., Gruber, N., Aumont, O., Bopp, L., Doney, S.C., Dunne, J.P., Hauck, J., John, J.G., Lima, I.D., Seferian, R. & Volker, C. (2016) Projected decreases in future marine export production: the role of the carbon flux through the upper ocean ecosystem. *Biogeosciences*, **13**, 4023-4047.

Litchman, E., Klausmeier, C.A., Miller, J.R., Schofield, O.M. & Falkowski, P.G. (2006) Multi-nutrient, multi-group model of present and future oceanic phytoplankton communities. *Biogeosciences*, **3**, 585-606.

Malick, M.J., Cox, S.P., Mueter, F.J. & Peterman, R.M. (2015) Linking phytoplankton phenology to salmon productivity along a north-south gradient in the Northeast Pacific Ocean. *Canadian Journal of Fisheries and Aquatic Sciences*, **72**, 697-708.

Mann, H.B. (1945) Nonparametric tests against trend. *Econometrica* **13**

Marchese, C., Albouy, C., Tremblay, J.-É., Dumont, D., D'Ortenzio, F., Vissault, S. & Bélanger, S. (2017) Changes in phytoplankton bloom phenology over the North Water (NOW) polynya: a response to changing environmental conditions. *Polar Biology*,

Marinov, I., Doney, S.C. & Lima, I.D. (2010) Response of ocean phytoplankton community structure to climate change over the 21st century: partitioning the effects of nutrients, temperature and light. *Biogeosciences*, **7**, 3941-3959.

820   Maritorena, S., d'Andon, O.H.F., Mangin, A. & Siegel, D.A. (2010) Merged satellite ocean color data
821   products using a bio-optical model: Characteristics, benefits and issues. *Remote Sensing of*
822   *Environment*, **114**, 1791-1804.
823   Martinez, E., Antoine, D., D'Ortenzio, F. & Montegut, C.D. (2011) Phytoplankton spring and fall blooms in
824   the North Atlantic in the 1980s and 2000s. *Journal of Geophysical Research-Oceans*, **116**
825   Moore, C.M., Mills, M.M., Arrigo, K.R., Berman-Frank, I., Bopp, L., Boyd, P.W., Galbraith, E.D., Geider,
826   R.J., Guieu, C., Jaccard, S.L., Jickells, T.D., La Roche, J., Lenton, T.M., Mahowald, N.M., Maranon,
827   E., Marinov, I., Moore, J.K., Nakatsuka, T., Oschlies, A., Saito, M.A., Thingstad, T.F., Tsuda, A. &
828   Ulloa, O. (2013) Processes and patterns of oceanic nutrient limitation. *Nature Geoscience*, **6**,
829   701-710.
830   Moran, X.A.G., Lopez-Urrutia, A., Calvo-Diaz, A. & Li, W.K.W. (2010) Increasing importance of small
831   phytoplankton in a warmer ocean. *Global Change Biology*, **16**, 1137-1144.
832   Mouw, C., Hardman-Mountford, N., Alvain, S., Bracher, A., Brewin, R., Bricaud, A., Ciotti, A., Devred, E.,
833   Fujiwara, A., Hirata, T., Hirawake, T., Kostadinov, T., Roy, S. & Uitz, J. (2017) A Consumer's Guide
834   to Satellite Remote Sensing of Multiple Phytoplankton Groups in the Global Ocean. *Frontiers in*
835   *Marine Science*, **4**
836   Mouw, C.B., Barnett, A., McKinley, G.A., Gloege, L. & Pilcher, D. (2016) Phytoplankton size impact on
837   export flux in the global ocean. *Global Biogeochemical Cycles*, **30**, 1542-1562.
838   Perry, R.I. (2011) Potential impacts of climate change on marine wild capture fisheries: an update.
839   *Journal of Agricultural Science*, **149**, 63-75.
840   Platt, T., Fuentes-Yaco, C. & Frank, K.T. (2003) Spring algal bloom and larval fish survival. *Nature*, **423**,
841   398-399.
842   Racault, M.F., Le Quere, C., Buitenhuis, E., Sathyendranath, S. & Platt, T. (2012) Phytoplankton
843   phenology in the global ocean. *Ecological Indicators*, **14**, 152-163.
844   Reigstad, M., Carroll, J., Slagstad, D., Ellingsen, I. & Wassmann, P. (2011) Intra-regional comparison of
845   productivity, carbon flux and ecosystem composition within the northern Barents Sea. *Progress*
846   *in Oceanography*, **90**, 33-46.
847   Reygondeau, G., Longhurst, A., Martinez, E., Beaugrand, G., Antoine, D. & Maury, O. (2013) Dynamic
848   biogeochemical provinces in the global ocean. *Global Biogeochemical Cycles*, **27**, 1046-1058.
849   Reynolds, R.W., Rayner, N.A., Smith, T.M., Stokes, D.C. & Wang, W.Q. (2002) An improved in situ and
850   satellite SST analysis for climate. *Journal of Climate*, **15**, 1609-1625.
851   Rodionov, S.N. (2004) A sequential algorithm for testing climate regime shifts. *Geophysical Research*
852   *Letters*, **31**, Doi 10.1029/2004gl019448.
853   Rodionov, S.N. (2006) Use of prewhitening in climate regime shift detection. *Geophysical Research*
854   *Letters*, **33**, Doi 10.1029/2006gl025904.
855   Roxy, M.K., Ritika, K., Terray, P. & Masson, S. (2014) The Curious Case of Indian Ocean Warming. *Journal*
856   *of Climate*, **27**, 8501-8509.
857   Roxy, M.K., Modi, A., Murtugudde, R., Valsala, V., Panickal, S., Kumar, S.P., Ravichandran, M., Vichi, M. &
858   Levy, M. (2016) A reduction in marine primary productivity driven by rapid warming over the
859   tropical Indian Ocean. *Geophysical Research Letters*, **43**, 826-833.
860   Ryther, J.H. (1969) Photosynthesis and fish production in the sea. *Science*, **166**, 72–76.
861   Sapiano, M.R.P., Brown, C.W., Uz, S.S. & Vargas, M. (2012) Establishing a global climatology of marine
862   phytoplankton phenological characteristics. *Journal of Geophysical Research-Oceans*, **117**
863   Schweigert, J.F., Thompson, M., Fort, C., Hay, D.E., Therriault, T.W. & Brown, L.N. (2013) Factors linking
864   Pacific herring (*Clupea pallasi*) productivity and the spring plankton bloom in the Strait of
865   Georgia, British Columbia, Canada. *Progress in Oceanography*, **115**, 103-110.
866   Siegel, D.A., Doney, S.C. & Yoder, J.A. (2002) The North Atlantic spring phytoplankton bloom and
867   Sverdrup's critical depth hypothesis. *Science*, **296**, 730-733.

868   Sigman, D.M. & Hain, M.P. (2012) The Biological Productivity of the Ocean. *Nature Education*, **3**, 1-16.

869   Soppa, M.A., Volker, C. & Bracher, A. (2016) Diatom phenology in the Southern Ocean: mean patterns,
870   trends and the role of climate oscillations. *Remote Sensing*, **8**

871   Stock, C.A., John, J.G., Rykaczewski, R.R., Asch, R.G., Cheung, W.W.L., Dunne, J.P., Friedland, K.D., Lam,
872   V.W.Y., Sarmiento, J.L. & Watson, R.A. (2017) Reconciling fisheries catch and ocean productivity.
873   *Proceedings of the National Academy of Sciences of the United States of America*, **114**, E1441-
874   E1449.

875   Taboada, F.G. & Anadon, R. (2014) Seasonality of North Atlantic phytoplankton from space: impact of
876   environmental forcing on a changing phenology (1998-2012). *Global Change Biology*, **20**, 698-
877   712.

878   Thomas, M.K., Kremer, C.T., Klausmeier, C.A. & Litchman, E. (2012) A global pattern of thermal
879   adaptation in marine phytoplankton. *Science*, **338**, 1085-1088.

880   Ueyama, R. & Monger, B.C. (2005) Wind-induced modulation of seasonal phytoplankton blooms in the
881   North Atlantic derived from satellite observations. *Limnology and Oceanography*, **50**, 1820-
882   1829.

883   Vazquez, D.P., Gianoli, E., Morris, W.F. & Bozinovic, F. (2017) Ecological and evolutionary impacts of
884   changing climatic variability. *Biological Reviews*, **92**, 22-42.

885   Visser, P.M., Verspagen, J.M.H., Sandrini, G., Stal, L.J., Matthijs, H.C.P., Davis, T.W., Paerl, H.W. &
886   Huisman, J. (2016) How rising CO2 and global warming may stimulate harmful cyanobacterial
887   blooms. *Harmful Algae*, **54**, 145-159.

888   Yamada, K. & Ishizaka, J. (2006) Estimation of interdecadal change of spring bloom timing, in the case of
889   the Japan Sea. *Geophysical Research Letters*, **33**

890   Zhang, M., Zhang, Y.L., Qiao, F.L., Deng, J. & Wang, G. (2017) Shifting trends in bimodal phytoplankton
891   blooms in the North Pacific and North Atlantic oceans from space with the Holo-Hilbert spectral
892   analysis. *Ieee Journal of Selected Topics in Applied Earth Observations and Remote Sensing*, **10**,
893   57-64.

894   Zhang, S., Harrison, M.J., Rosati, A. & Wittenberg, A. (2007) System design and evaluation of coupled
895   ensemble data assimilation for global oceanic climate studies. *Monthly Weather Review*, **135**,
896   3541-3564.

897

Table 1 Pearson product-moment correlation between mean relative Theil-Sen slope binned by 5° latitude and longitude groupings of bloom parameters start day, magnitude, intensity, and duration and abiotic factors sea surface temperature, salinity, mixed layer depth, zonal wind stress, and meridional wind stress. Significant correlations shown in bold.

		SST		Salinity		MLD		u-wind		v-wind	
		r	p	r	p	r	p	r	p	r	p
Latitude	Start	0.173	0.429	0.159	0.447	-0.103	0.626	0.034	0.872	0.014	0.946
	Magnitude	0.345	0.107	0.336	0.100	0.201	0.334	-0.230	0.269	*-0.576*	*0.003*
	Intensity	*0.576*	*0.004*	*0.428*	*0.033*	0.386	0.056	-0.265	0.200	*-0.571*	*0.003*
	Duration	*-0.656*	*0.001*	-0.128	0.543	-0.241	0.246	0.075	0.722	0.091	0.665
Longitude	Start	-0.074	0.534	0.185	0.117	*0.303*	*0.009*	-0.116	0.327	*-0.364*	*0.002*
	Magnitude	0.066	0.579	*0.334*	*0.004*	*0.338*	*0.003*	0.124	0.298	0.053	0.654
	Intensity	0.026	0.826	0.210	0.074	*0.286*	*0.014*	0.006	0.960	0.224	0.057
	Duration	0.072	0.547	*0.382*	*0.001*	*0.239*	*0.042*	*0.343*	*0.003*	-0.193	0.101

Figure 1 Global map showing the extent of 1° latitudinal/longitudinal grid locations with at least 10 years with detected blooms color coded by eight subdivisions of the world ocean. Latitude limits of tropical subdivisions approximate the Tropic of Cancer and Capricorn. Red stippling marks grid locations representing oligotrophic ocean areas.
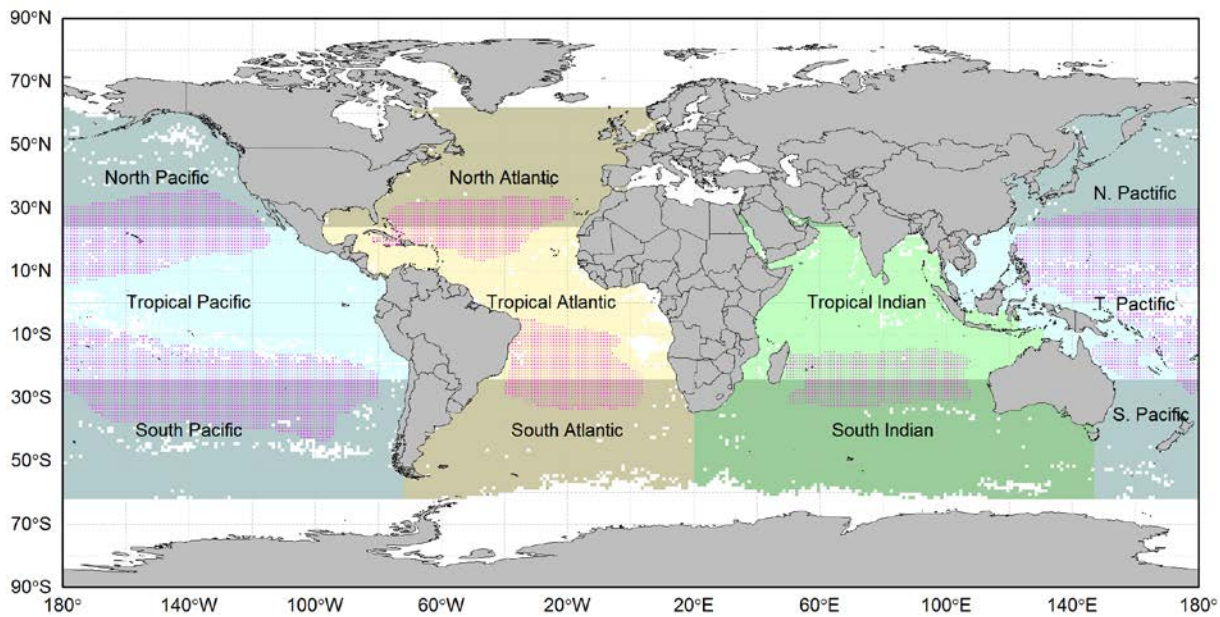
Figure 2 Bloom frequency (a), start day (b), magnitude (c), and duration (d) for the dominant annual bloom based on a global 1° latitudinal/longitudinal grid over the study period 1998-2015. Units: bloom frequency (percentage); bloom start day (day of the year), Day/Date: 50/Feb 19, 100/Apr 9, 150/May 29, 200/Jul 18, 250/Sep 6, 300/Oct 26, 350/Dec 15; bloom magnitude [log (mg m^{-3} 8-day+1)]; and, bloom duration (days).
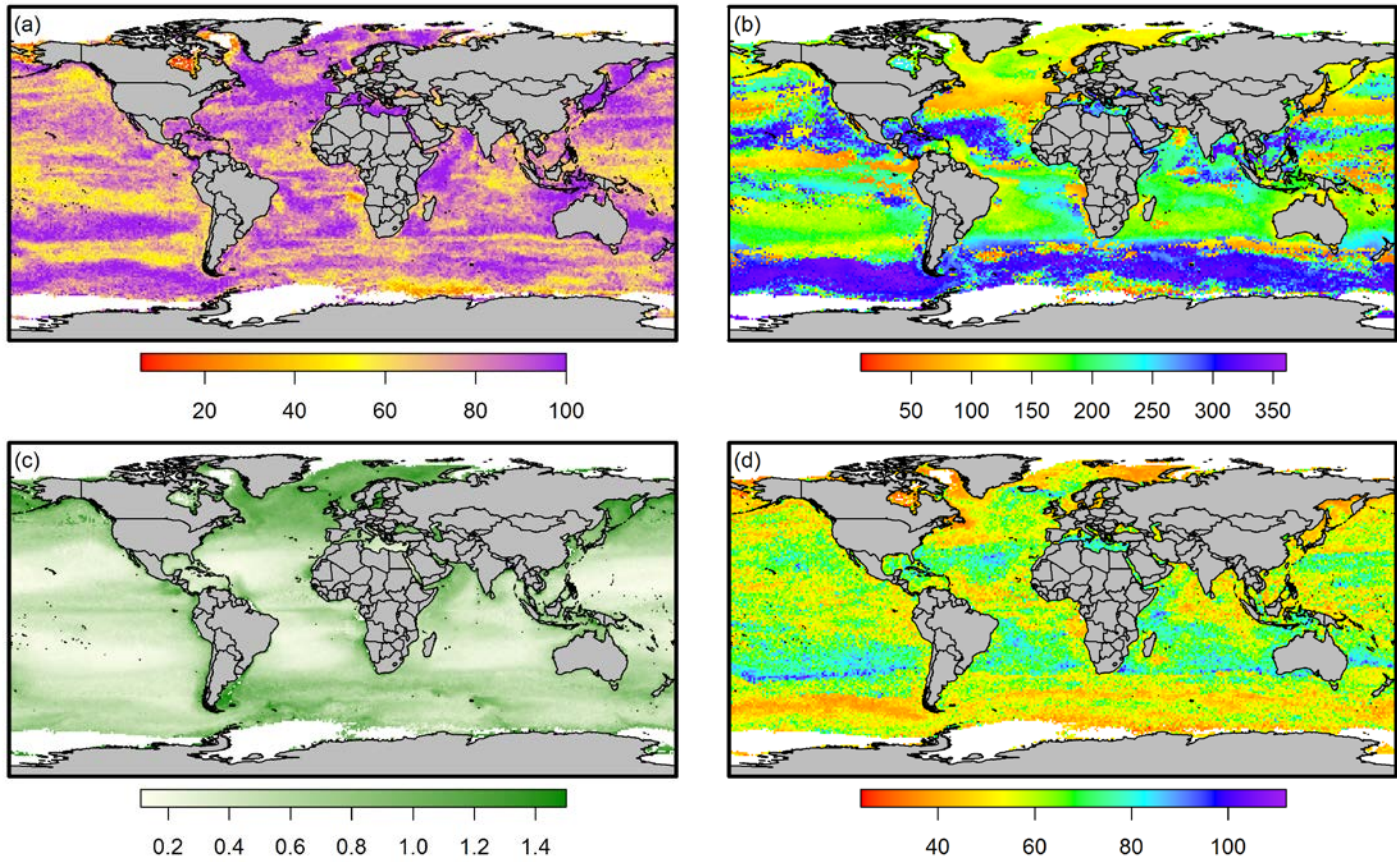
Figure 3 Correlation between bloom start day and duration (a), magnitude (b), and intensity (c) for the dominant annual bloom based on a global 1° latitudinal/longitudinal grid over the study period 1998-2015. Only grid locations with at least eight years with detected blooms were included; red makers indicate significant negative correlations (ρ<0.05), blue makers indicate significant positive correlations, and beige markers indicate non-significant correlations.
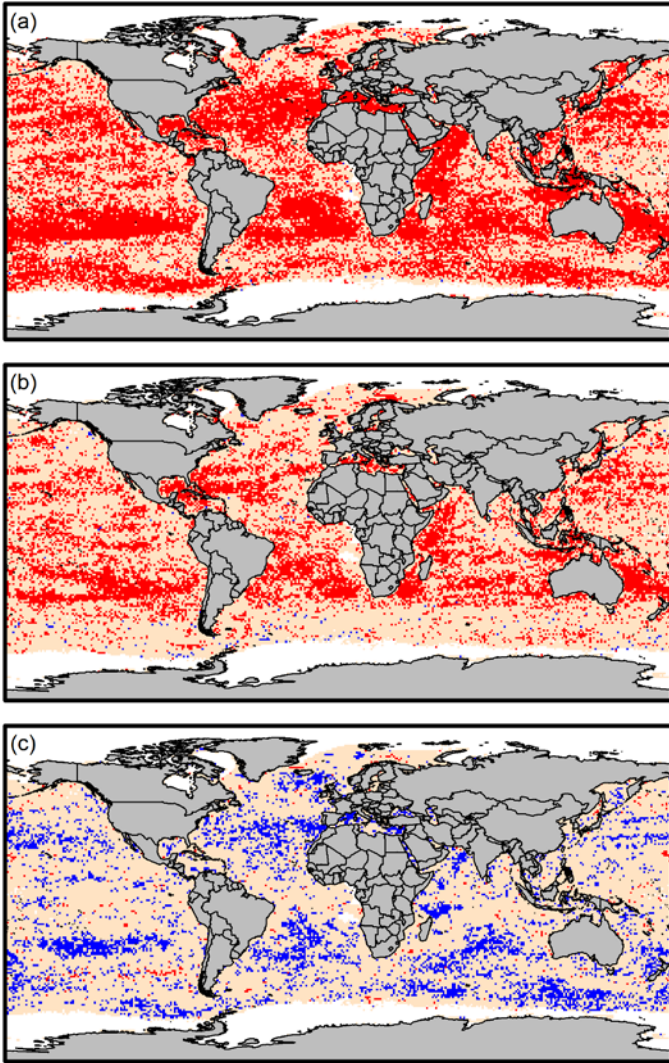
Figure 4 Relative Theil-Sen slope showing time series trends in start day (a), magnitude (b), intensity (c), and duration (d) for the dominant annual bloom based on a global 1° latitudinal/longitudinal grid over the study period 1998-2015. Only grid locations with at least ten years with detected blooms were included. Blue shades denote positive change and red denote negative change.
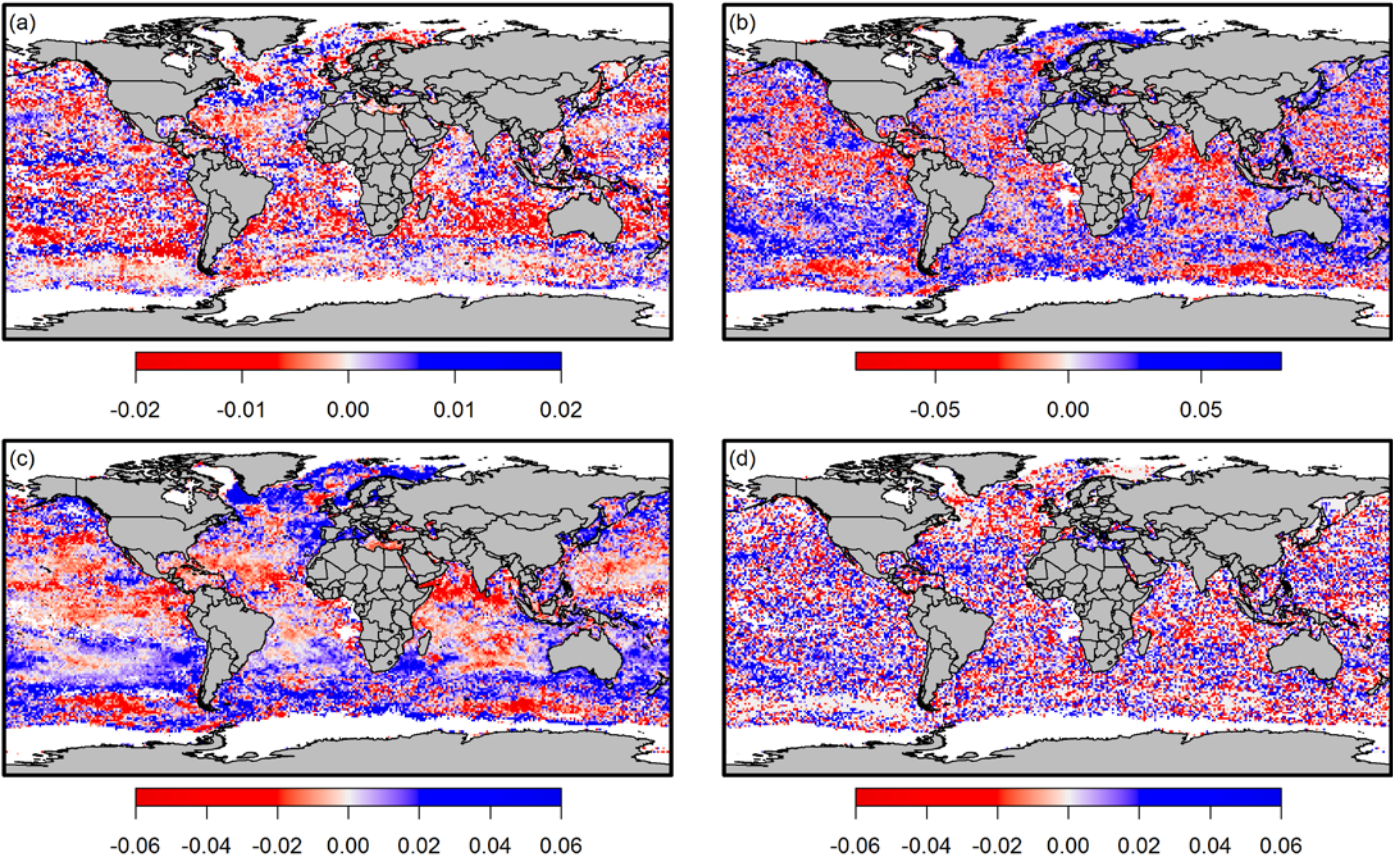
Figure 5 Mean annual relative Theil-Sen slope binned by 5° latitude and longitude groupings showing time series trends in start day (a and b, respectively), magnitude (c and d, respectively), intensity (e and f, respectively), and duration (g and h, respectively) for the dominant annual bloom based on a global 1° latitudinal/longitudinal grid over the study period 1998-2015. Only grid locations with at least ten years of detected blooms were included. Error bars are 95% confidence intervals and gray lines are LOESS smoothers using a span setting of 0.5.
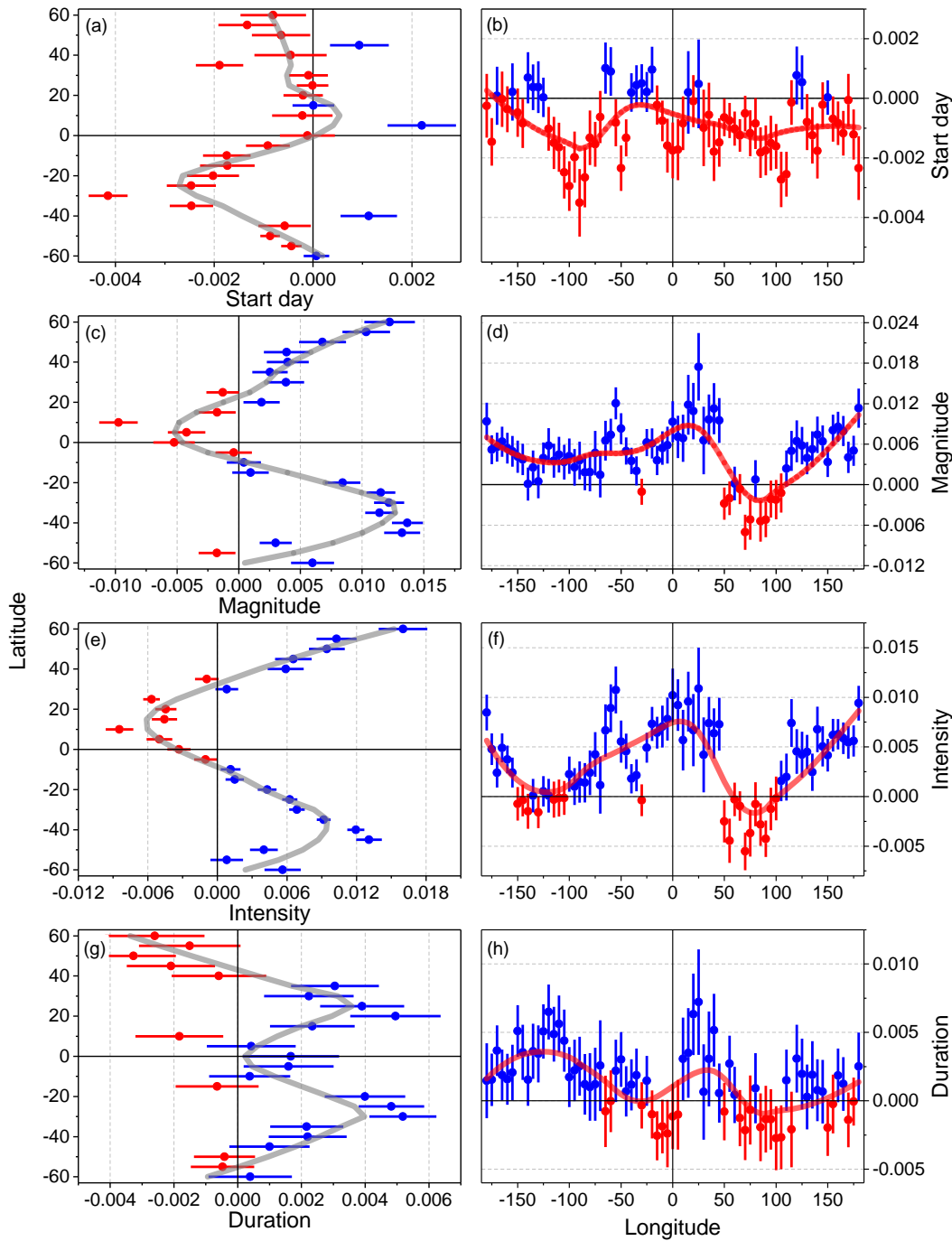
Figure 6. Relative Theil-Sen slope showing time series trends in sea surface temperature (a), salinity (b), mixed layer depth (c), zonal wind stress (d), and meridional wind stress (e) based on a global 1° latitudinal/longitudinal grid over the study period 1998-2015.
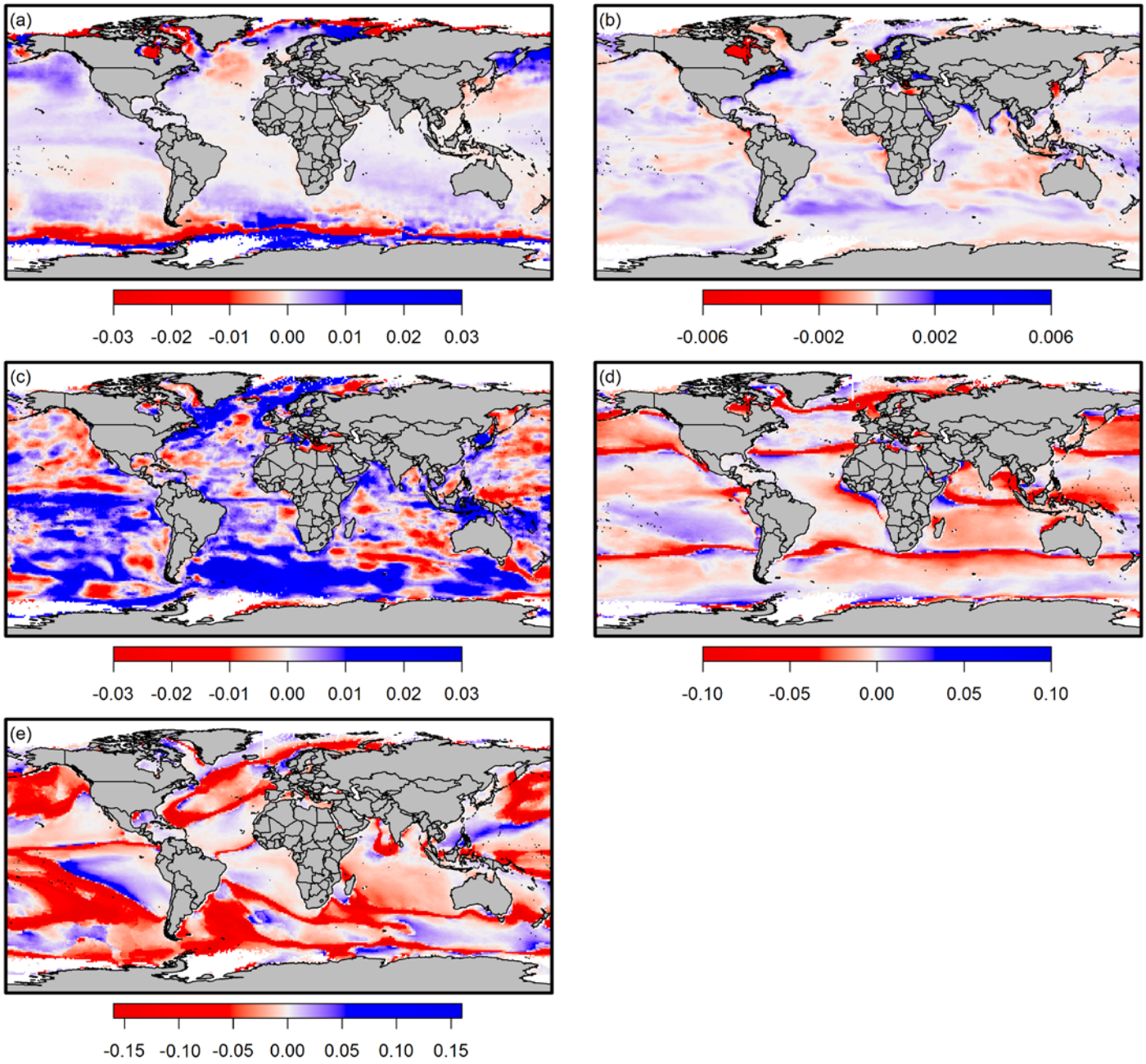
Figure 7. Mean annual relative Theil-Sen slope binned by 5° latitude and longitude groupings showing time series trends in SST (a and b, respectively), salinity (c and d, respectively), mixed layer depth (e and f, respectively), zonal wind stress (g and h, respectively), and meridional wind stress (i and j, respectively) for the dominant annual bloom based on a global 1° latitudinal/longitudinal grid over the study period 1998-2015. Only grid locations with at least ten years of detected b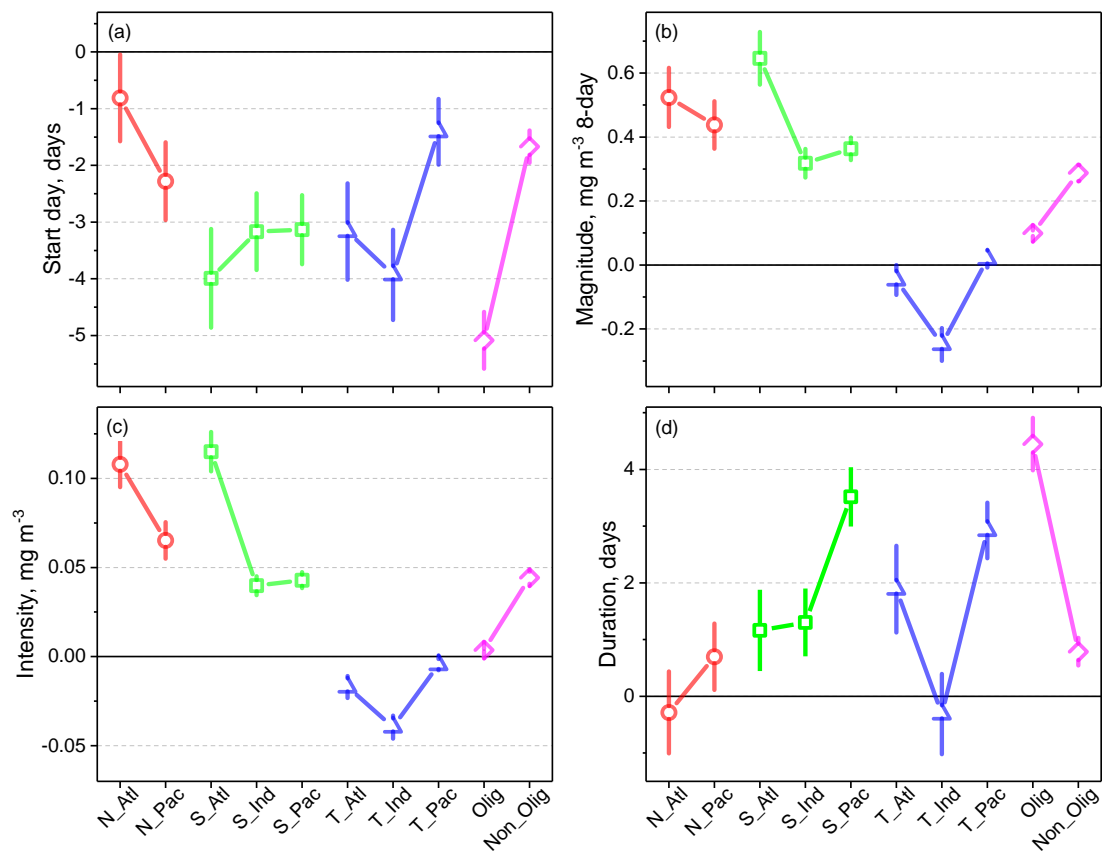looms were included. Error bars are 95% confidence intervals and gray lines are LOESS smoothers using a span setting of 0.5.
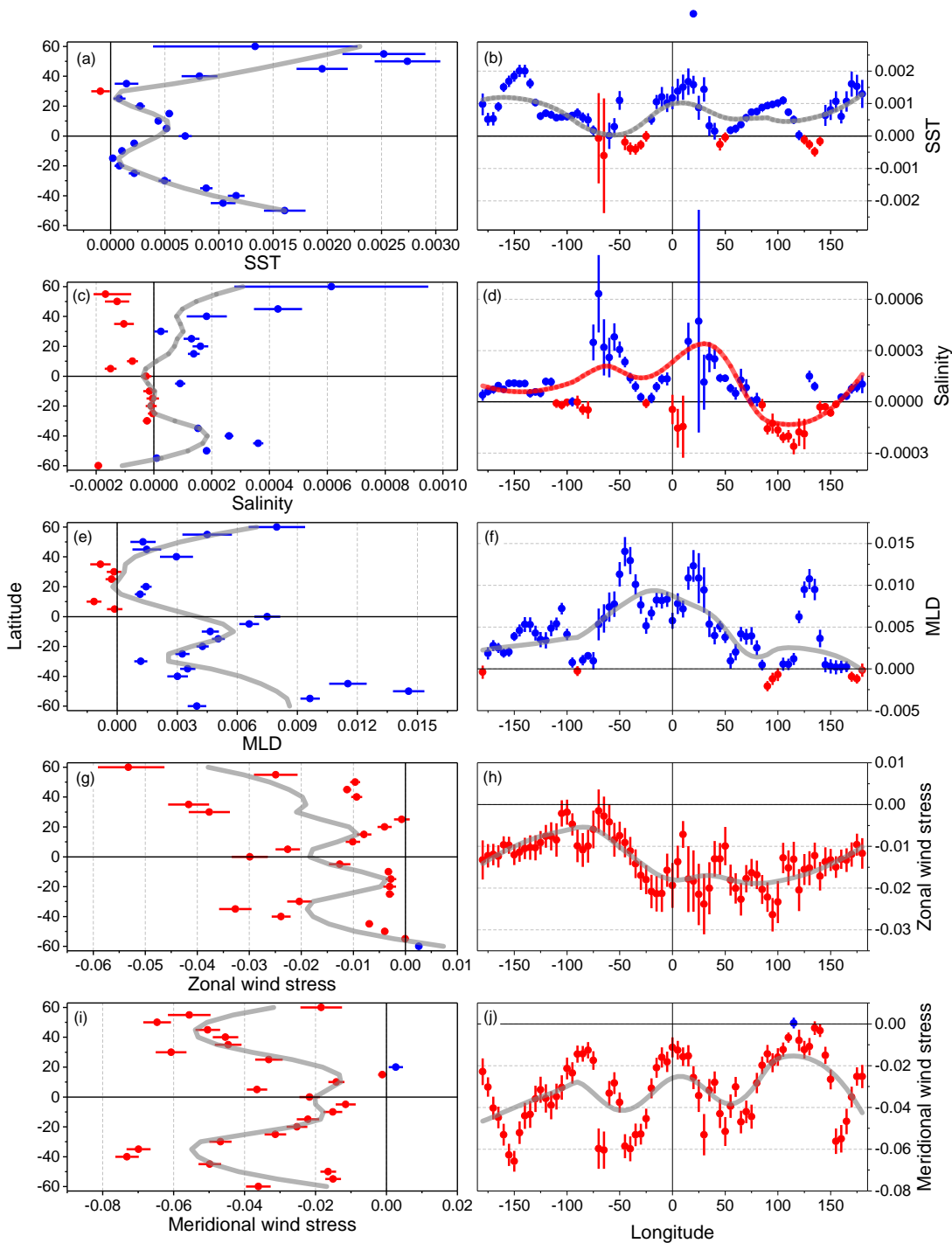
Figure 8 Mean global interval and cumulative absolute trends in bloom start day (a), magnitude (b), intensity (c), and duration (d) versus Mann-Kendall trend test probability intervals. Trends are the product of Theil-Sen slopes for the dominant annual bloom and the number of years in the time series. Probability interval 0.0 includes p<0.05, interval 0.1 includes 0.05≤p<0.15, etc. Each interval estimate includes trends associated with that interval probability level only and are estimated from all data excluding outliers. Cumulative trends are based on data from the interval trends and all lower probability intervals. Only grid locations with at least ten years with detected blooms were included based on a global 1° latitudinal/longitudinal grid over the study period 1998-2015 excluding data from latitudes north and south of 62°N and 62°S, respectively. Error bar are 95% confidence intervals.
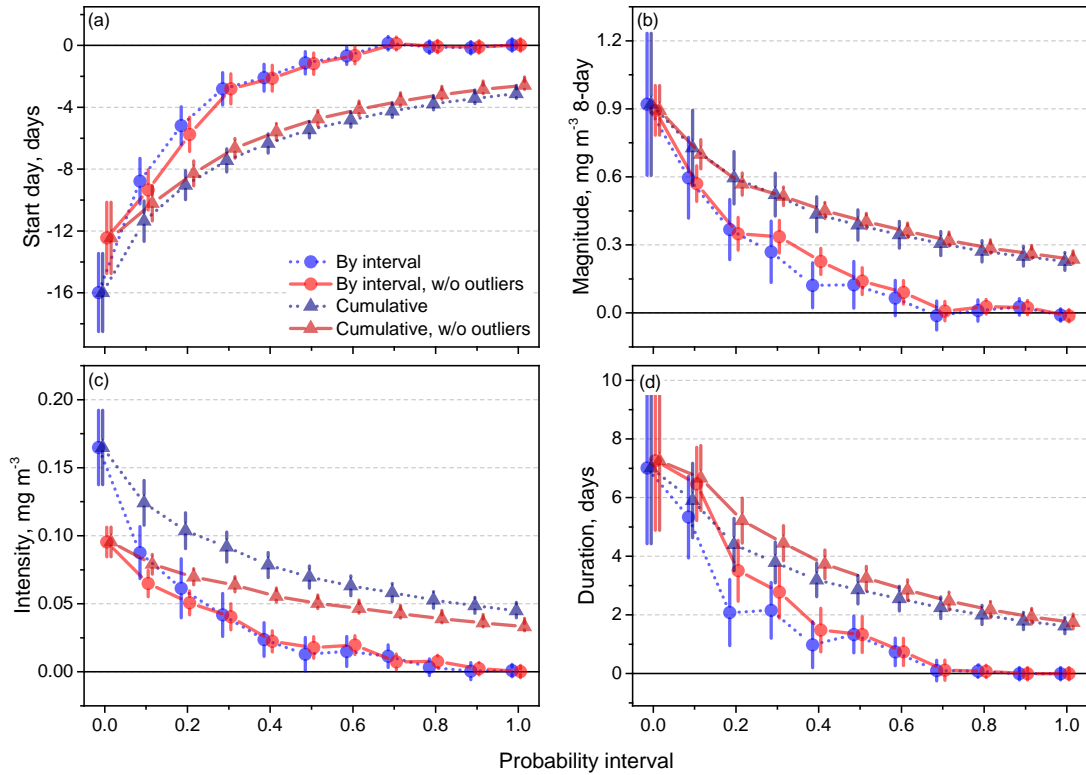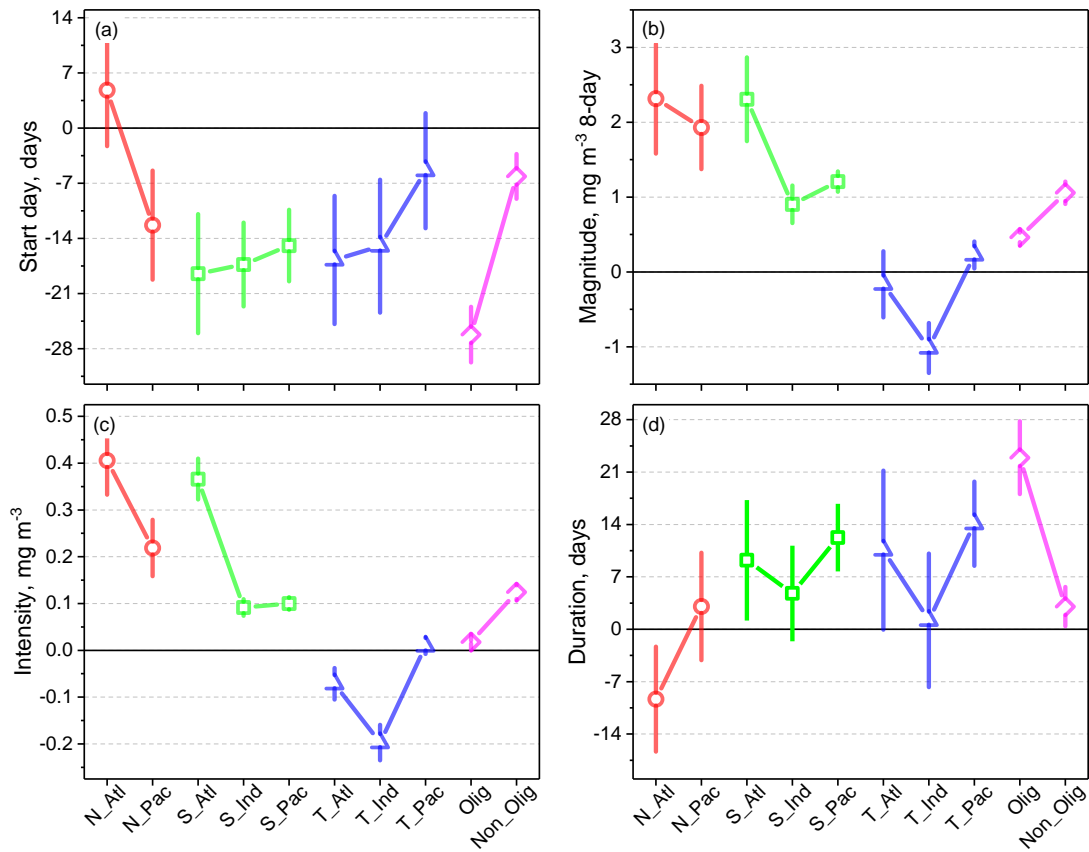
Figure 9 Mean absolute trends over ocean areas for bloom start day (a), magnitude (b), intensity (c), and duration (d) for areas regardless of significance level (all p-levels). Trends are the product of Theil-Sen slopes for the dominant annual bloom and the number of years in the times series based on a global 1° latitudinal/longitudinal grid over the study period 1998-2015 excluding data from latitudes north of 62°N and south of 62°S. Grid locations are combined as per ocean areas and oligotrophic versus non-oligotrophic area as per figure 1 [N_Atl, N_Pac = North Atlantic and Pacific (red circles); S_Atl, S_Ind, S_Pac = South Atlantic, Indian, and Pacific (green squares); T_Atl, T_Ind, T_Pac = Tropical Atlantic, Indian, and Pacific (blue triangles); Olig, Non-Olig = Oligotrophic and Non-Oligotrophic areas (magenta diamonds)]. Only grid locations with at least ten years with detected blooms were included and outliers were excluded. Error bar are 95% confidence intervals.

Figure 10 Mean absolute trends over ocean areas for bloom start day (a), magnitude (b), intensity (c), and duration (d) for areas with significant trends (p<0.05). Trends are the product of Theil-Sen slopes for the dominant annual bloom and the number of years in the times series based on a global 1° latitudinal/longitudinal grid over the study period 1998-2015 excluding data from latitudes north of 62°N and south of 62°S. Grid locations are combined as per ocean areas and oligotrophic versus non-oligotrophic area as per figure 1 [N_Atl, N_Pac = North Atlantic and Pacific (red circles); S_Atl, S_Ind, S_Pac = South Atlantic, Indian, and Pacific (green squares); T_Atl, T_Ind, T_Pac = Tropical Atlantic, Indian, and Pacific (blue triangles); Olig, Non-Olig = Oligotrophic and Non-Oligotrophic areas (magenta diamonds)]. Only grid locations with at least ten years with detected blooms were included and outliers were excluded. Error bar are 95% confidence intervals.

Supporting information

Short Title: Bloom intensity.

Appendix S1 Bloom intensity [log (mg m^{-3}+1)] for the dominant annual bloom based on a global 1° latitudinal/longitudinal grid over the study period 1998-2015.
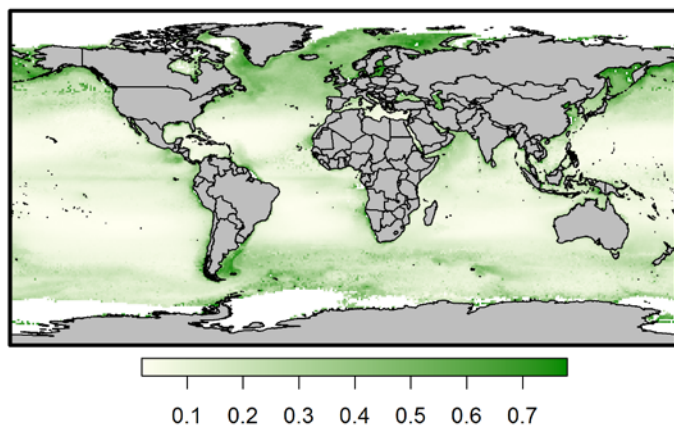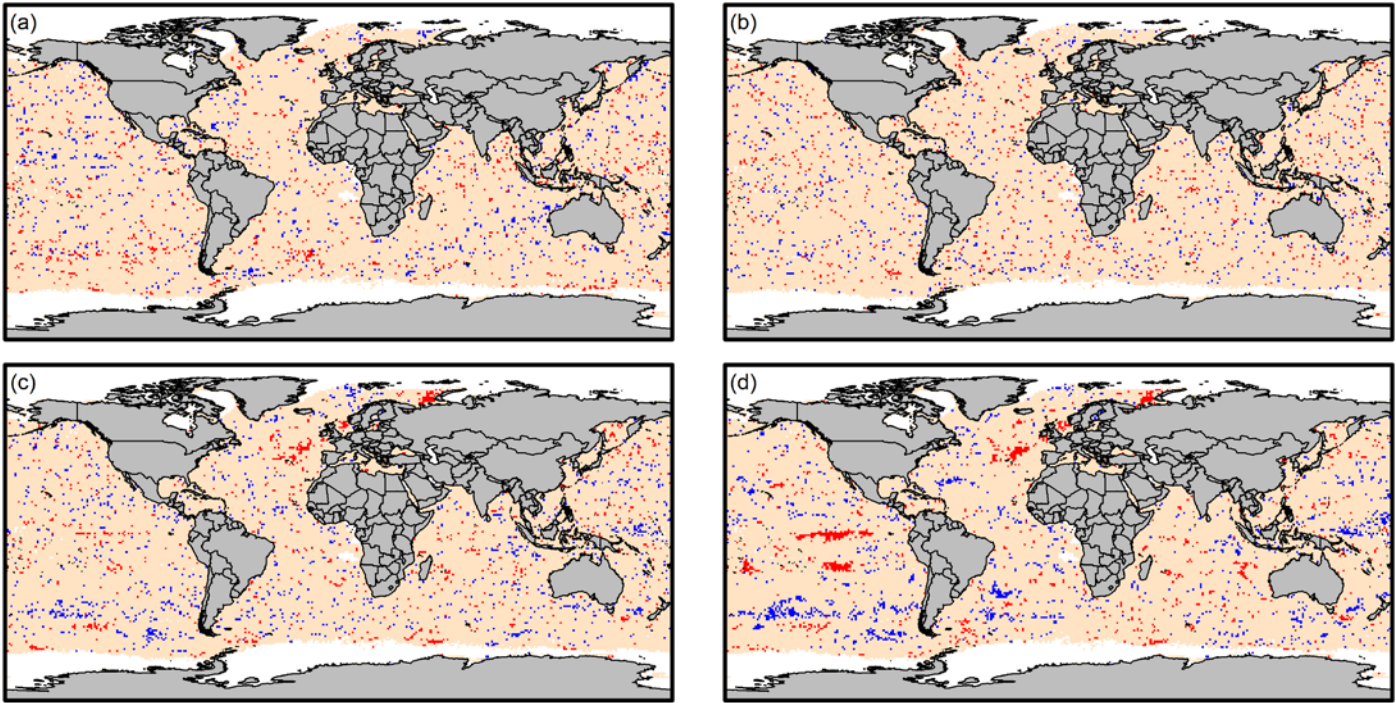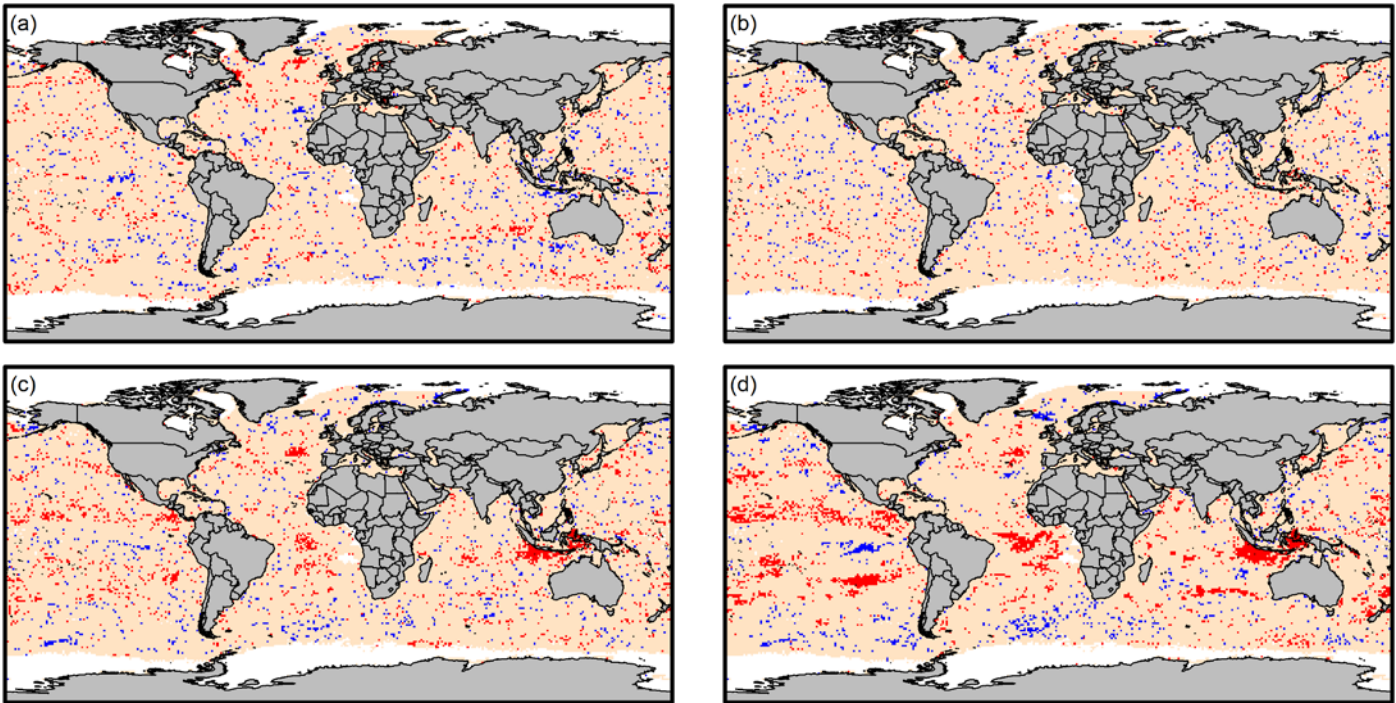
Figure s2-1. Correlation between monthly SST and bloom start day (a), duration (b), magnitude (c), and intensity (d) for the dominant annual bloom based on a global 1° latitudinal/longitudinal grid over the study period 1998-2015. Only grid locations with at least eight years with detected blooms were included; red makers indicate significant negative correlations ($\rho<0.05$), blue makers indicate significant positive correlations, and beige markers indicate non-significant correlations.
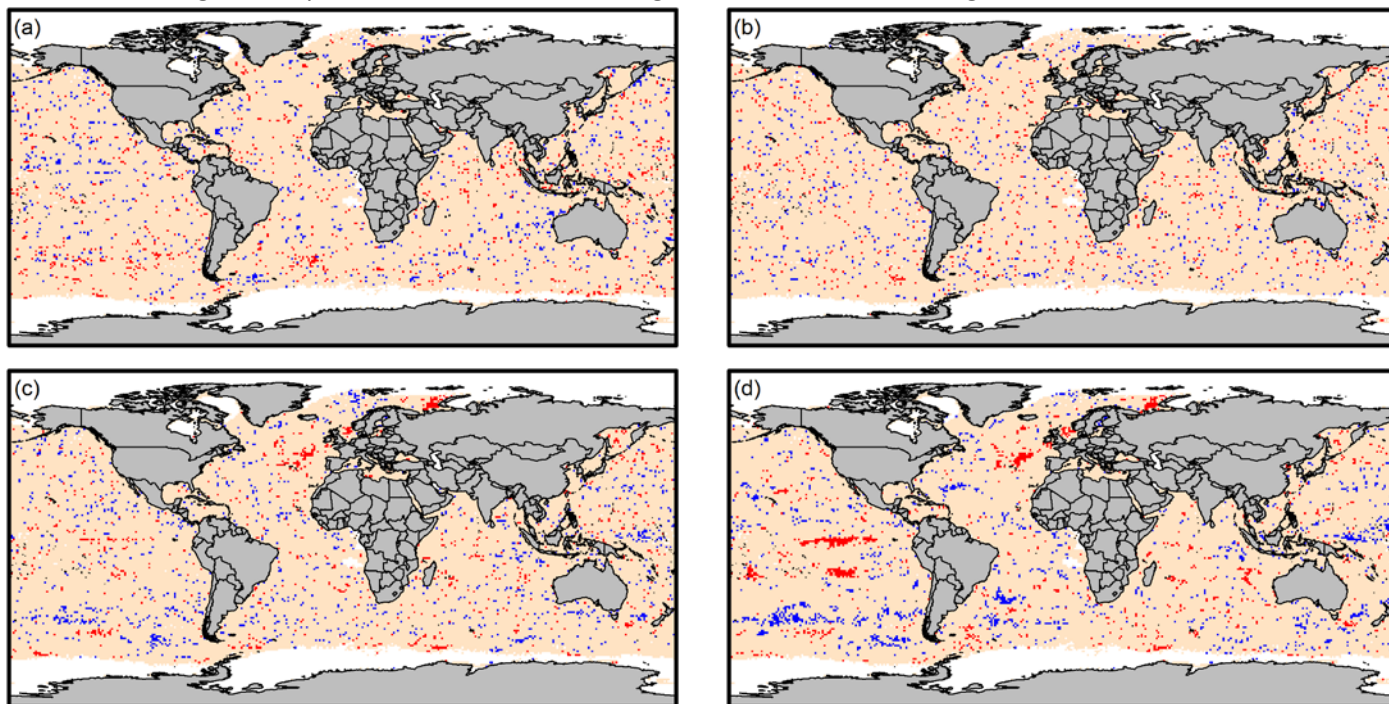

Figure s2-2. Correlation between annual mean SST and bloom start day (a), duration (b), magnitude (c), and intensity (d) for the dominant annual bloom based on a global 1° latitudinal/longitudinal grid over the study period 1998-2015. Only grid locations with at least eight years with detected blooms were included; red makers indicate significant negative correlations ($\rho<0.05$), blue makers indicate significant positive correlations, and beige markers indicate non-significant correlations.

Figure s2-3. Correlation between monthly salinity and bloom start day (a), duration (b), magnitude (c), and intensity (d) for the dominant annual bloom based on a global 1° latitudinal/longitudinal grid over the study period 1998-2015. Only grid locations with at least eight years with detected blooms were included; red makers indicate significant negative correlations (ρ<0.05), blue makers indicate significant positive correlations, and beige markers indicate non-significant correlations.

Figure s2-4. Correlation between mean annual salinity and bloom start day (a), duration (b), magnitude (c), and intensity (d) for the dominant annual bloom based on a global 1° latitudinal/longitudinal grid over the study period 1998-2015. Only grid locations with at least eight years with detected blooms were included; red makers indicate significant negative correlations (ρ<0.05), blue makers indicate significant positive correlations, and beige markers indicate non-significant correlations.
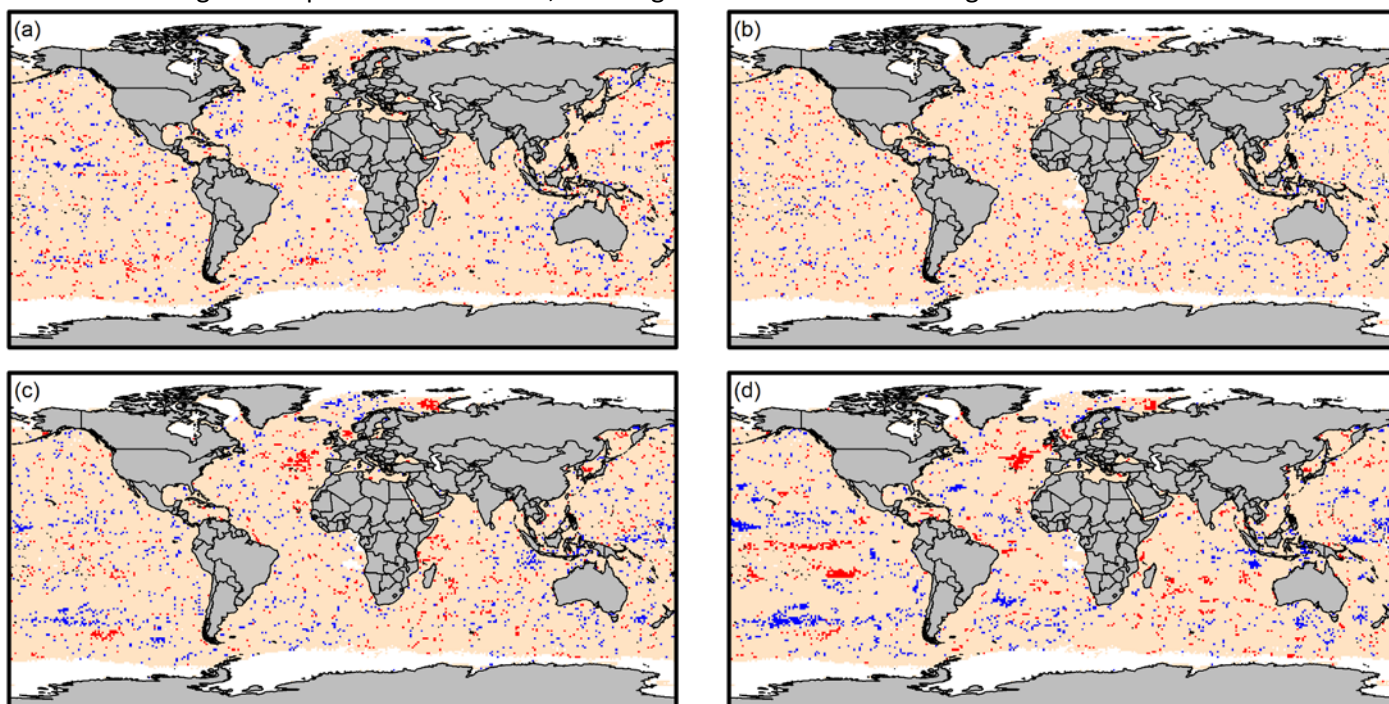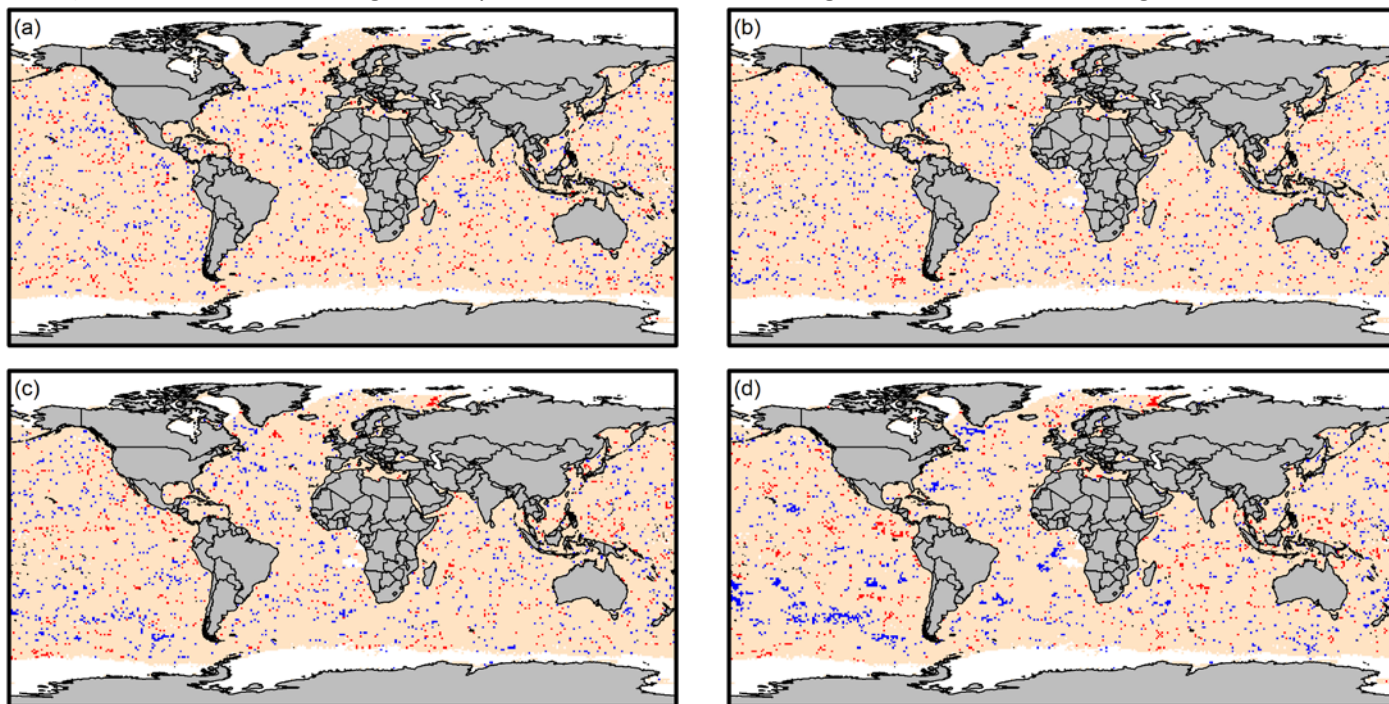
Figure s2-5. Correlation between monthly mixed layer depth and bloom start day (a), duration (b), magnitude (c), and intensity (d) for the dominant annual bloom based on a global 1° latitudinal/longitudinal grid over the study period 1998-2015. Only grid locations with at least eight years with detected blooms were included; red makers indicate significant negative correlations (ρ<0.05), blue makers indicate significant positive correlations, and beige markers indicate non-significant correlations.

Figure s2-6. Correlation between mean annual mixed layer depth and bloom start day (a), duration (b), magnitude (c), and intensity (d) for the dominant annual bloom based on a global 1° latitudinal/longitudinal grid over the study period 1998-2015. Only grid locations with at least eight years with detected blooms were included; red makers indicate significant negative correlations (ρ<0.05), blue makers indicate significant positive correlations, and beige markers indicate non-significant correlations.
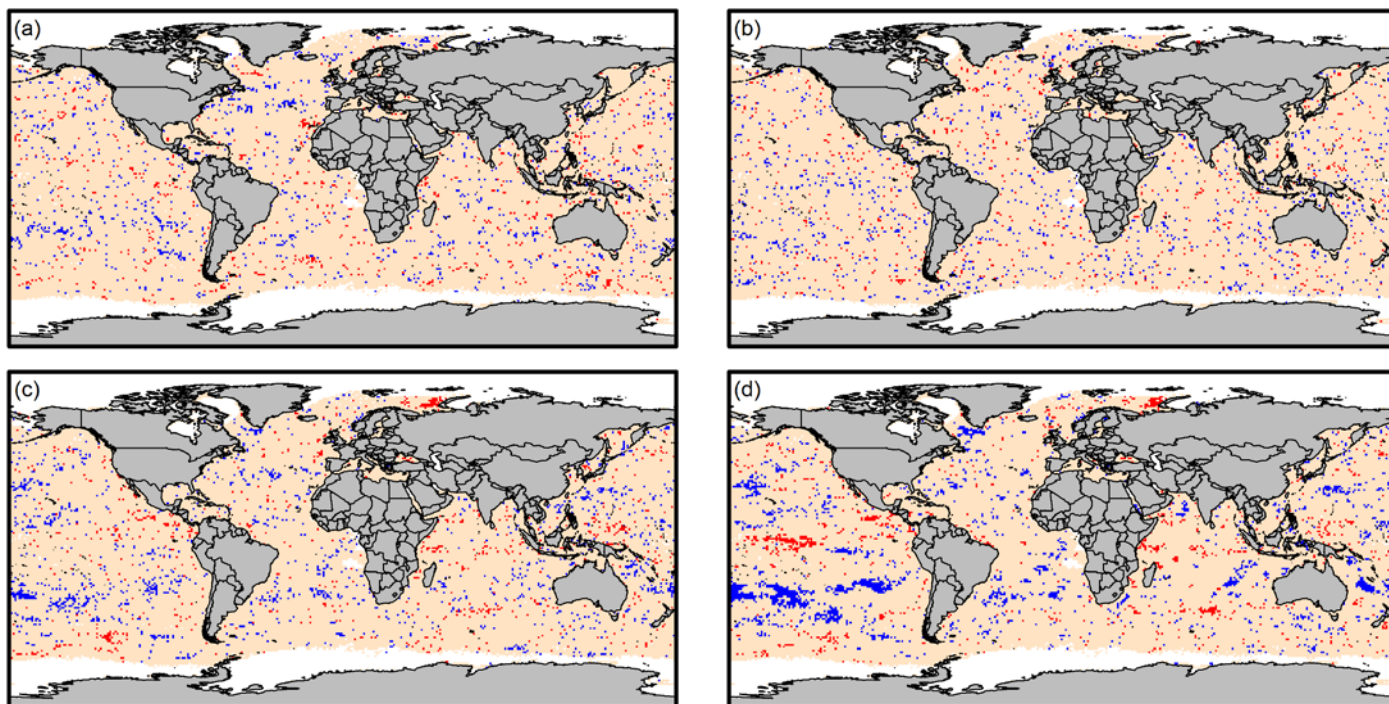
Figure s2-7. Correlation between monthly u-vector wind stress and bloom start day (a), duration (b), magnitude (c), and intensity (d) for the dominant annual bloom based on a global 1° latitudinal/longitudinal grid over the study period 1998-2015. Only grid locations with at least eight years with detected blooms were included; red makers indicate significant negative correlations (ρ<0.05), blue makers indicate significant positive correlations, and beige markers indicate non-significant correlations.
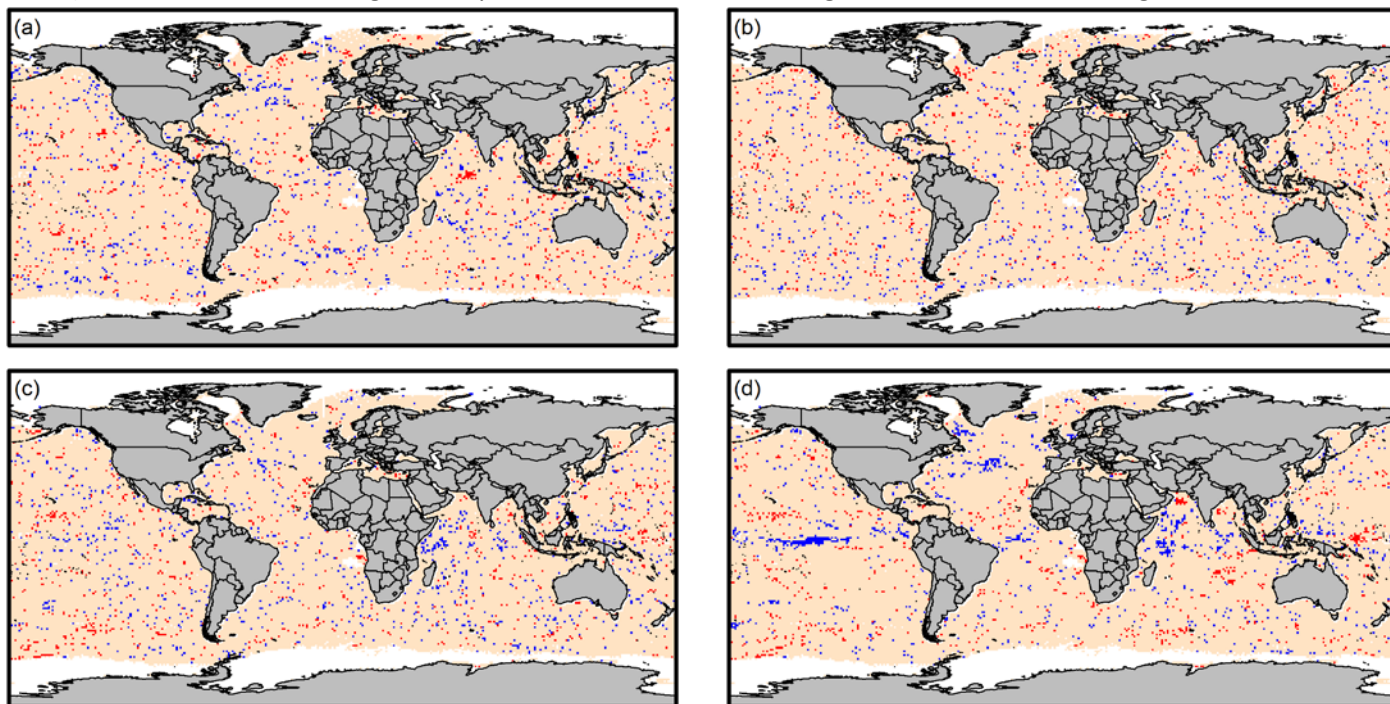

Figure s2-8. Correlation between mean annual u-vector wind stress and bloom start day (a), duration (b), magnitude (c), and intensity (d) for the dominant annual bloom based on a global 1° latitudinal/longitudinal grid over the study period 1998-2015. Only grid locations with at least eight years with detected blooms were included; red makers indicate significant negative correlations (ρ<0.05), blue makers indicate significant positive correlations, and beige markers indicate non-significant correlations.
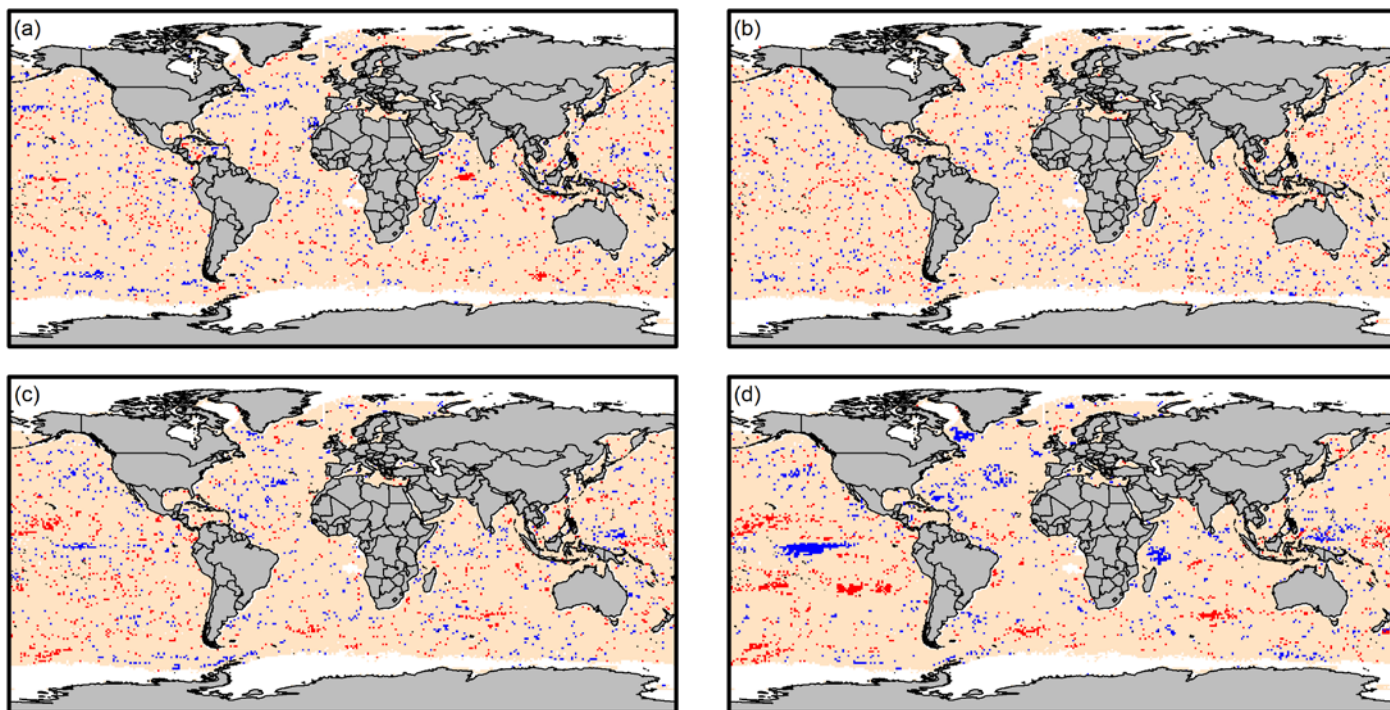
Figure s2-9. Correlation between monthly v-vector wind stress and bloom start day (a), duration (b), magnitude (c), and intensity (d) for the dominant annual bloom based on a global 1° latitudinal/longitudinal grid over the study period 1998-2015. Only grid locations with at least eight years with detected blooms were included; red makers indicate significant negative correlations (ρ<0.05), blue makers indicate significant positive correlations, and beige markers indicate non-significant correlations.
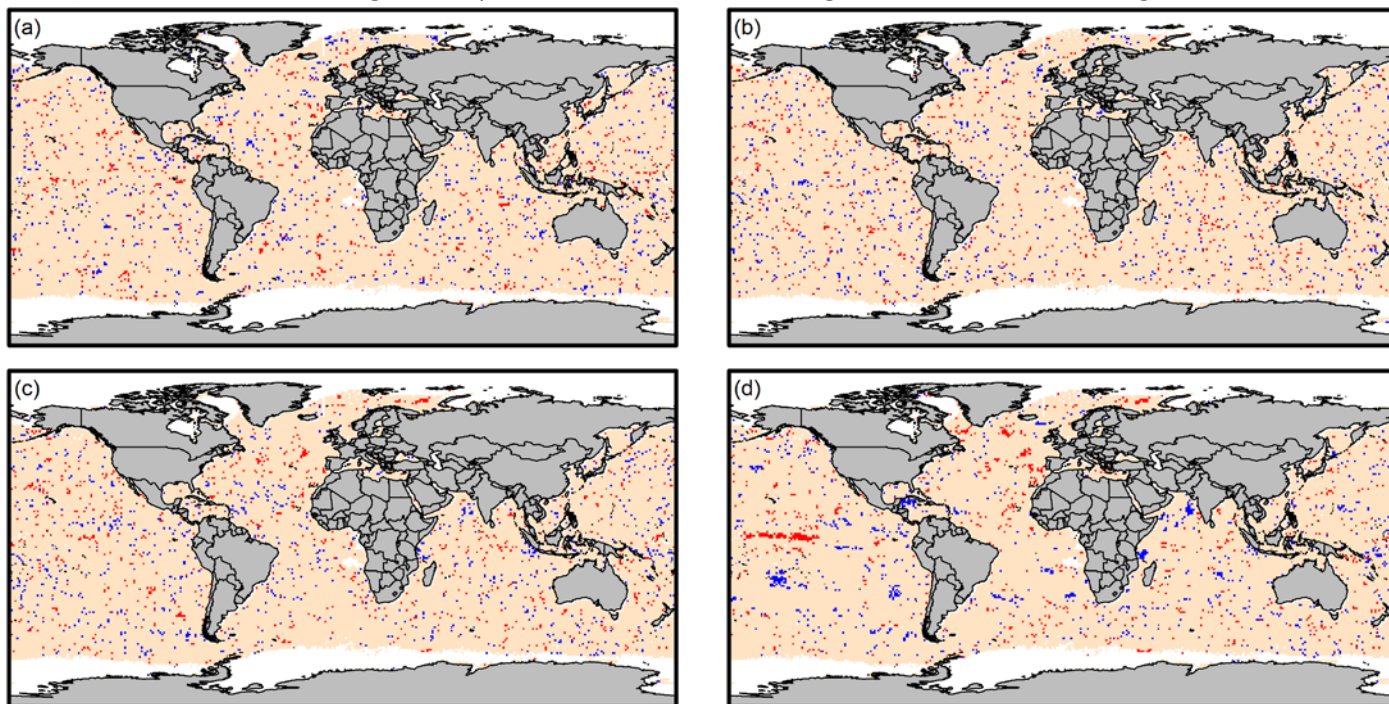

Figure s2-10. Correlation between mean annual v-vector wind stress and bloom start day (a), duration (b), magnitude (c), and intensity (d) for the dominant annual bloom based on a global 1° latitudinal/longitudinal grid over the study period 1998-2015. Only grid locations with at least eight years with detected blooms were included; red makers indicate significant negative correlations (ρ<0.05), blue makers indicate significant positive correlations, and beige markers indicate non-significant correlations.